



UNIVERSITY OF HELSINKI

<https://helda.helsinki.fi>

## **Using the Taguchi experimental design for assessing within-field variability of surface run-off and soil erosion risk**

**Raza, Ahsan; Ahrends, Hella Ellen; Habib-ur-Rahman, Muhammed; Hueging, Hubert; Gaiser, Thomas**

**2022-07-01**

Elsevier B.V.

<http://hdl.handle.net/10138/573340>

Raza, A, Ahrends, H E, Habib-ur-Rahman, M, Hueging, H & Gaiser, T 2022, 'Using the Taguchi experimental design for assessing within-field variability of surface run-off and soil erosion risk', *Science of the Total Environment*, vol. 828, 154567. <https://doi.org/10.1016/j.scitotenv.2022.154567>

Downloaded from Helda, University of Helsinki institutional repository. <https://helda.helsinki.fi>  
This is an electronic reprint of the original article.  
This reprint may differ from the original in pagination and typographic detail.  
Please cite the original version.

1 **Using the Taguchi experimental design for assessing within-field variability of surface run-**  
2 **off and soil erosion risk**

3 **Ahsan Raza<sup>1,\*</sup>, Hella Ahrends<sup>2</sup>, Muhammad Habib-ur-Rahman<sup>1</sup>, Hubert Hüging<sup>1</sup> and Thomas Gaiser<sup>1</sup>**

4 <sup>1</sup>**University of Bonn, Institute of Crop Science and Resource Conservation (INRES), Crop Science Group,**  
5 **Katzenburgweg 5, 53115, Bonn, Germany**

6 <sup>2</sup>**University of Helsinki, Department of Agricultural Sciences, 00014 Helsinki, Finland;**

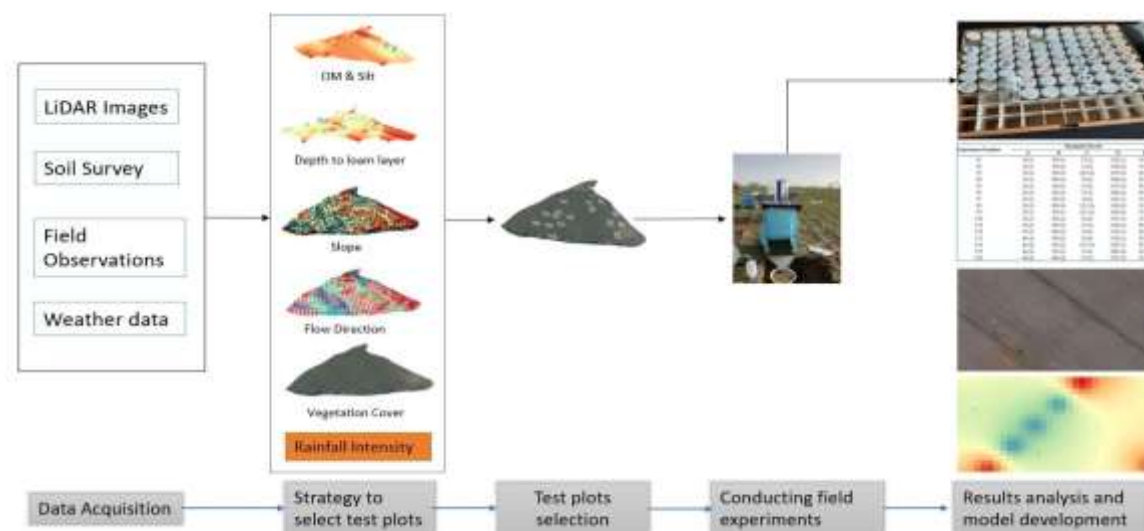
7 **\*Correspondence: araza@uni-bonn.de; Tel.: +49(0)228 73-7200**

8 **Highlights**

- 9 • Taguchi’s Fractional factorial experiment design approach was used to rank the factors affecting  
10 within-field soil erosion  
11 • Signal-to-noise ratio analysis was used to identify optimum conditions for maximum sediment  
12 yield, runoff, and carbon and nitrogen content of sediments.  
13 • Rainfall intensity contributed most strongly to erosion processes with 40.6 % followed by  
14 the slope (23.8 %).  
15 • Applied workflow allowed for efficiently predicting soil erosion and identifying areas susceptible  
16 to soil loss at a high spatial resolution

17

18 **Graphical abstract**



19

20 **Keywords:** Design of experiment, heterogeneous field conditions, rainfall simulator, erosion-prone areas

21

22

23 **Abstract**

24 Water erosion is one of the soil degradation processes driven by environmental and field factors  
25 such as rainfall intensity, slope gradient, dynamics of vegetation cover, soil characteristics, and  
26 management practices. Most of the studies assess the separate contribution of these factors under  
27 controlled conditions. However, there is a lack of adequate knowledge regarding the complex  
28 interactions between prevailing factors and soil erosion processes under heterogeneous field  
29 conditions. This study investigated 16 combinations of 5 factors at 4 levels of each factor on the  
30 soil erosion process using Taguchi's fractional factorial experiment design, identifying the factor  
31 combinations resulting in maximum sediment yield, runoff, organic carbon, and nitrogen losses.  
32 We considered the factors: Soil organic matter and silt content (SiltOM), vegetation cover (VC),  
33 slope steepness (SS), rainfall intensity (RI), and depth to a loamy layer (DLL). The interactive  
34 effects of these factors and their combinations were visualized from the analysis of signal-to-noise  
35 (S/N) responses. Results indicated that interactions between the selected factors and soil erosion  
36 processes exist and multiple linear regression models were developed to predict sediment yields,  
37 runoff, carbon, and nitrogen losses at the sub-field scale. Results revealed that 1) RI with 40.6 %  
38 showed the highest contribution to sediment yield followed by SS (23.8 %), VC (17.74 %), SiltOM  
39 (14.77 %), and DLL (3.17 %), indicating a strong rainfall-erosion relationship; 2) the combination  
40 of levels of factors generating highest sediment yield was determined; 3) A simple multiple linear  
41 regression model developed for predicting local sediment yield showed the highest agreement with  
42 field observations ( $R^2=82.5$  %). The findings suggest that Taguchi design could be used reliably  
43 for modeling soil erosion at field and sub-field scales. Using local calibration data such models  
44 have great potential for soil erosion risk assessments at the field scale, especially in areas where  
45 contributing factors and factor levels change at small spatial scales.

46

47

48

49

50

51

## 52        **1. Introduction**

53        Soil erosion by water has become a great concern all over the world (Keating et al., 2003;  
54        Krysanova et al., 2007). Soil erosion has significant impacts on environmental sustainability by  
55        adversely influencing agricultural production, water quality, and natural resources conservation  
56        (Issaka and Ashraf, 2017). It reduces the fertile soil depth and crop available soil moisture by the  
57        removal of essential nutrients and soil organic matter (SOM) and hence reducing the productivity  
58        of the soil (Jahun et al., 2015). Soil erosion by water is a form of land degradation resulting from  
59        multiple factors with complex interactions. Among others, these factors are rainfall intensity,  
60        runoff, small-scale soil heterogeneity in the vertical and horizontal direction, topography, and  
61        temporal variability of crop conditions (Václavík et al., 2013). Affected by heterogeneous  
62        environmental and field conditions, soil erosion involves complex processes that can strongly vary  
63        within single fields, in particular in undulated areas. (Cerdan et al., 2010). Therefore, identifying  
64        and categorizing the main causes of soil erosion at the field scale based on observations with a high  
65        spatial resolution for quantitatively assessing the spatial and temporal variability of soil erosion  
66        patterns are of great importance. Such information can provide support for decision-making for  
67        improved sub-field management and for farmers to avoid the degradation of fertile soils and for  
68        maintaining or enhancing crop productivity.

69        Numerous experimental and modeling studies have been conducted using approaches ranging from  
70        analytical to empirical techniques to gain a better understanding of runoff and soil erosion  
71        processes (Raza et al., 2021) and their potential outcomes (organic carbon and nitrogen losses, soil  
72        depth reduction, etc.) under heterogeneous field conditions (Aga et al., 2020; Eslamian, 2014; J.  
73        R. Williams et al., 1984; Knisel and Nicks, 1981; Syvitski and Kettner, 2008; Viney and Sivapalan,  
74        1999). Individual hydro-geomorphological processes and vegetation dynamics affect the soil  
75        erosion process differently depending on the scale (Aga et al., 2020; Nearing et al., 1999; Panagos  
76        and Katsoyiannis, 2019). In particular, soil physical properties such as soil structure, texture, bulk  
77        density, compaction, and soil thickness influence the erosion pattern and thus rate and magnitude  
78        of erosion (Ouyang et al., 2018; Ramezanpour et al., 2010). Other driving factors are the  
79        topography (i.e., slope gradient, slope length) and ground cover, which modify the physical forces  
80        and greatly impact hydrological processes (Liu and Singh, 2004). The amount, intensity, and  
81        frequency of precipitation are critical meteorological factors for surface runoff generation and soil  
82        erosion.

83 A few authors investigated the interactive impact of environmental and soil conditions on soil  
84 erosion. (Guidry et al., 2006; Sepaskhah and Bazrafshan-Jahromi, 2006) investigated the runoff  
85 and soil erosion under rainfall, varying slope, and soil factors, and found that the potentialities of  
86 both surface runoff and sediment yield varied with the level of rainfall erosivity but the impact  
87 differed among soil textures and slopes, indicating diverse nonlinearities of rainfall-runoff-soil  
88 factors-erosion relationships and their complex interaction. (Zambon et al., 2021) studied the  
89 dependency of soil erosion on soil surface conditions (seal formation) and soil types under  
90 controlled rainfall intensities. Under the same initial surface conditions, the erosion development  
91 for increasing rainfall intensity was almost consistent. (Warrington et al., 1989) noticed that  
92 increasing slope inclination tends to increase erosion, whereas removing surface crusts and  
93 increasing permeability rate led to decreasing surface runoff. (Gross et al., 1991) concluded that  
94 even low density vegetation coverage noticeably decreases the sediment yield with increasing  
95 rainfall intensities. However, different studies yield a different representation of erosion processes  
96 Differences in the results of the studies are mainly caused by the particular experimental conditions  
97 (selection of factors) and set-ups which affected the output. To date, there are a few attempts made  
98 to study the impact of multiple environmental and in-field factors to predict sediment yield and  
99 runoff, including, in some cases, carbon, and nitrogen losses under natural conditions (Anh et al.,  
100 2014; Li et al., 2017; J. H. Zhang et al., 2015). Most of these studies consider only one (Cerdà et  
101 al., 2021; Dunjón et al., 2004) or two (Ouyang et al., 2018; Ramos et al., 2019) factors to explain  
102 the erosion process and ignore the complex interaction of potential factors and specifically their in-  
103 field variability that may strongly affect the sediment yield and surface runoff. Most of these studies  
104 used defined rainfall intensities at plot scales to investigate soil erosion using a rainfall simulator.

105 Rainfall simulators and soil erosion plots are two widely used research facilities to assess and  
106 quantify the processes of soil erosion and sediment transport in overland flow (Sharpley and  
107 Kleinman, 2003). Different types of rainfall simulators with their specifications and sizes being  
108 optimized for specific pedo-climatic zones, topographies and land uses have been successfully  
109 applied in several field experiments (Barthès and Roose, 2002; Duiker et al., 2001; Fernández-  
110 Gálvez et al., 2008; Guidry et al., 2006; Lasanta et al., 2000; M. Sheklabadi et al., 2012; Sepaskhah  
111 and Bazrafshan-Jahromi, 2006; Srinivasan et al., 2007). However, many of these studies used  
112 standard plot sizes under controlled conditions (Albaladejo Montoro and Stocking, 1989; Raza et  
113 al., 2021; Renard et al., 1991) and with rainfall intensities far higher than the threshold for soil

114 detachment thus neglecting the interactions of modulated intensities and soil characteristics that  
115 can drive fine-scale spatial soil erosion processes (Kusumandari et al., 2021; Poulénard et al.,  
116 2001). In summary, there is still a lack of knowledge on the interactive effects of multiple factors  
117 and their potential levels on soil erosion processes under natural conditions that explicitly consider  
118 sub-field scale spatio-temporal dynamics. The quantitative knowledge is however of great  
119 importance for agricultural fields where management activities can lead to changes in the  
120 vulnerability of soils to erosion. Spatially explicit knowledge will help to understand within-field  
121 dynamics of erosion and sedimentation and greatly support precision agriculture by developing  
122 physical-based on empirical-based models. . Further, it provides quantitative validation data for  
123 high-resolution remote sensing data (such as unmanned aerial vehicle (UAV)-based Lidar  
124 measurements).

125 Most of the previous studies were conducted under controlled conditions with a limited number of  
126 factors, factor levels, and their interactions (Liu et al., 2019; Rieke-Zapp and Nearing, 2005;  
127 Sadeghi et al., 2017; Yusuf et al., 2016). Observing multiple factors and their complex interactions  
128 requires establishing several field experiments to disentangle their effects on spatial variation in  
129 soil erosion. Therefore, these studies used full factorial experimental designs to investigate the  
130 magnitude of the effects of factors on soil erosion that require a large sample size because it  
131 increases exponentially when all combinations of factors, factor levels, and interactions are  
132 considered (L. D. Meyer, 1981; Li et al., 2019; Meyer and Harmon, 1989). These designs are not  
133 applicable when the number of experimental runs is limited due to their cost- and labor intensity.  
134 To handle this challenge, the Taguchi method can be applied to any experimental study where the  
135 effect of up to ~30 factors on processes is studied while labor and cost intensity are minimized  
136 without lowering the quality of outputs (Taguchi, 1986). The Taguchi method is a type of general  
137 fractional factorial design, based on a selected number of factors and factor levels to identify the  
138 least number of experiments to be performed without compromising the overall output (Taguchi,  
139 1987, 1986). So far, in an agricultural context, the Taguchi design mainly has been used for  
140 investigating the impact of fertilizer rates and plant density on cotton yields (Awty-Carroll et al.,  
141 2020; Chou et al., 2010; Ruchika Deo et al., 2007; Sivaiah & Chakradhar, 2019b). Further, it has  
142 been successfully applied to study soil erosion processes (Sadeghi et al. 2012, Mhaske et al. 2019)  
143 and results indicate similar performance compared with full factorial designs (Zhang et al. 2015,  
144 Zhang et al. 2021) and response surface methods (Moosavi & Sadeghi. 2021(F. Zhang et al.,

145 2015)). While providing evidence for the suitability of the design to study the effect of multiple  
146 factors on soil erosion, these studies only used a limited number of factors and their interactions.  
147 Further, runoff volume and resulting nutrient losses such as organic carbon and nitrogen from the  
148 field, which are critical variables for sustainable agriculture, were not investigated.

149 Encouraged by the successful application of this design in the studies mentioned above, we here  
150 use the Taguchi design to study fine-scale spatio-temporal dynamics of soil erosion processes  
151 (surface runoff, sediment yield, carbon and nitrogen losses) as affected by multiple factors at an  
152 agricultural field located in Western Europe under temperate climate conditions. More specifically,  
153 the objectives of this study are to

- 154 i. Investigate the within-field variability of the effects of the interaction between soil  
155 characteristics (soil organic matter (SOM), soil texture), topography (slope), rainfall  
156 intensity, and soil cover (field conditions) on soil erosion, surface runoff, carbon and  
157 nitrogen losses
- 158 ii. Quantify the percentage contribution of each of these five factors to soil erosion, surface  
159 runoff, carbon and nitrogen losses
- 160 iii. Develop empirical models to predict local runoff, sediment yield, carbon and nitrogen  
161 losses
- 162 iv. Identify erosion risk and sediment yield zones within the field

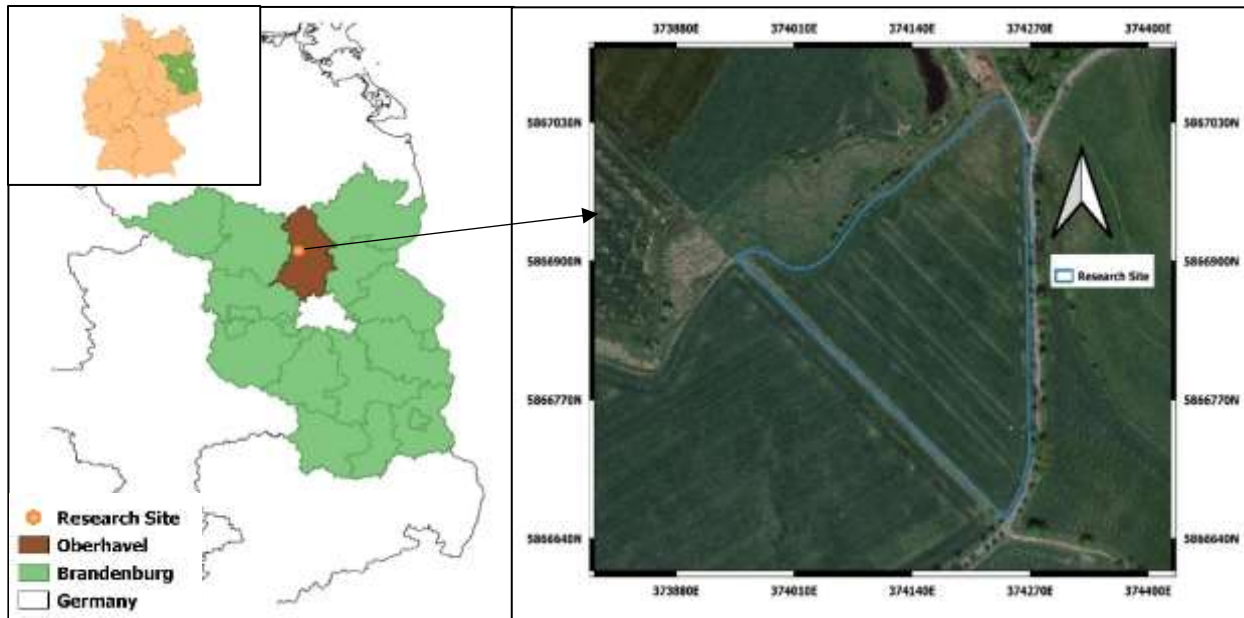
## 163 **2. Methodology**

### 164 2.1. Study area

165 The study was conducted on an agricultural field site located in the Löwenberger Land  
166 municipality, in the north of the federal state of Brandenburg, Germany (33U 374170E 5866893N)  
167 (Fig. 1). Brandenburg lies in the temperate, continental climate zone with mean annual  
168 temperatures between 7.8 °C and 9.5 °C and mean annual precipitation of ~ 600 mm (German  
169 Weather Service 2020, Ihinegbu & Ogunwumi, 2021). The research field comprises ~ 6.25 ha (Fig.  
170 1). Terrain height averages around 51.5 to 57.5 m a.s.l. with north east facing gentle slope (Fig.  
171 2). The soil was classified as Ferric Luvisol at up slopes (WRB, 2007) and in the marginal areas of  
172 the depression as Gley-Kolluvisol (Gleyic Anthrosol).

173

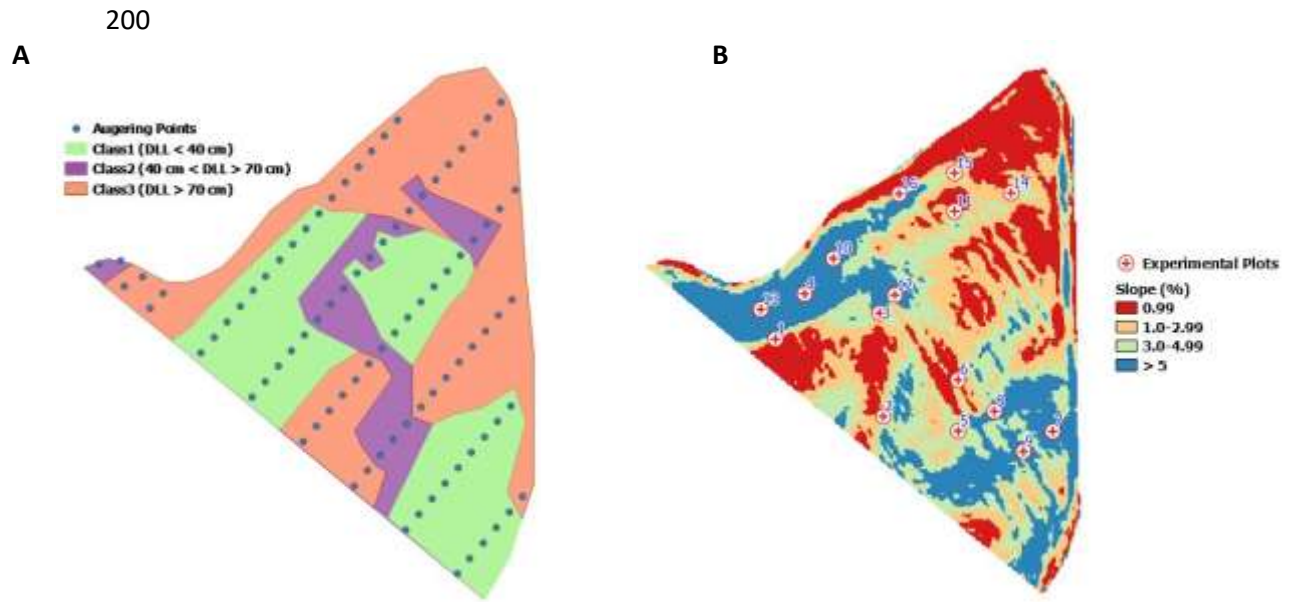
174



185 **Fig. 1: Location of the study area (left) and an aerial image of the research field (May 8<sup>th</sup>,**  
 186 **2020, Google Earth)**

187 2.2. Soil sampling

188 To characterize the spatial heterogeneity of soil characteristics soil augers (100 cm depth) were  
 189 obtained from 87 different locations within the field (Fig. 2) in December 2019. At selected points,  
 190 soil samples were analyzed for soil texture (proportion of silt, sand, and clay fractions) and SOM  
 191 content, and the depth from the soil surface to a loamy layer. In soils derived from glacial deposits,  
 192 the thickness of the sandy topsoil layers that are followed by a loamy layer, restricting vertical  
 193 water movement compared to the sandy topsoil, is considered to increase the risk of water ponding  
 194 at the soil surface and hence the risk of surface runoff and erosion. Samples were air-dried and  
 195 sieved through a 2 mm mesh. Particle size distribution was determined with the Pipett method after  
 196 SOM and carbonate destruction. Soil texture varied from silty loam to silt and medium sand  
 197 according to the German soil taxonomy. According to Hofmann et al. (2016) and the soil taxation  
 198 values in the German field cadastre of the state of Brandenburg (BB ATKIS), however, the topsoil  
 199 is dominated by loamy sand.



201 **Fig. 2: Study site with soil augering points (A) and the locations of the rainfall simulation**  
 202 **experimental plots (B, Numbers 1 to 16)**  
 203

204 2.3. Experimental design

205 In contrast to classical statistical designs the “Taguchi design” is a type of general fractional  
 206 factorial design, based on a selected number of factors and factor levels to identify the least number  
 207 of experiments to be performed (Taguchi, 1987, 1986). The main factors and interactions that are  
 208 most likely to be significant and the levels at which they are varied have to be defined in advance.  
 209 Based on this knowledge Taguchi orthogonal arrays are selected with the choice depending on the  
 210 tradeoff between time, resources, and quality of outputs (Medan et al., 2017; Rafidah et al., 2014;  
 211 Woll & Burkhard, 2005). Subsequently to the experimental runs, the effect of each variable can be  
 212 studied based on the signal-to-noise ratio (SN) (i.e., maximizing or minimizing SN ratios).

213 The Taguchi method systematically yields the best possible combination of factors and their levels  
 214 to produce quality output at lower experimental cost and time. Based on the literature review  
 215 (Chmelová and Šarapatka, 2002; P.U. et al., 2017; Pandey et al., 2007; Raza et al., 2021), For this  
 216 study, five factors were selected: Sum of the percentage of silt and soil organic matter (SiltOM),  
 217 vegetation cover (VC), slope steepness (SS), rainfall intensity (RI), and depth to loamy layer  
 218 (DLL). For each factor, four levels are considered (Table 1). The ranges of these levels are based  
 219 on soil surveys, site-specific scheduling of crop residue management (affecting vegetation cover),  
 220 and the field topography derived from 2008 Lidar data with 1m spatial resolution

221 (<https://geobroker.geobasis-bb.de>). The selection of rainfall intensity levels is based on an analysis  
 222 of 10-minute precipitation data provided by the German Weather Service for a nearby  
 223 meteorological station (Brandenburg weather station (ID # 3552)) and adjusted to the capability  
 224 and sensitivity of the mobile rainfall simulator (described below).

225 **Table 1: Experimental factors and their levels**

Factor	Description	Unit	Level 1	Level 2	Level 3	Level 4
1	(SiltOM)*	%	> 20	18 - 20	16 - 18	< 16
2	vegetation cover	%	1 - 5 (C)	0 (B)	10 - 15 (E)	> 15 (L)
3	Slope steepness	%	< 1	1-3	3-5	> 5
4	Rainfall intensity	mm min <sup>-1</sup>	< 2.5	2.7 - 3.3	3.4 - 4	> 4
5	Depth to loamy layer	cm	< 40	40 - 55	55 - 70	> 70

226 \*the % of SiltOM decreases from level 1 to level 4, decided based on laboratory soil texture  
 227 analysis. C, B, E, and L represent field conditions as cultivation, seedbed preparation, plant  
 228 emergence, and Leaf development stage (3 Leaves unfold) respectively.

229 Due to the number of factors (5) and levels (4) as defined in Table 1, the orthogonal array L<sub>16</sub> (4<sup>5</sup>)  
 230 for the Taguchi DOE was selected consisting of 16 experiments (factor combinations) (Table 2).

231

232

233

234

235

236

237

238

239

240

241

242

243

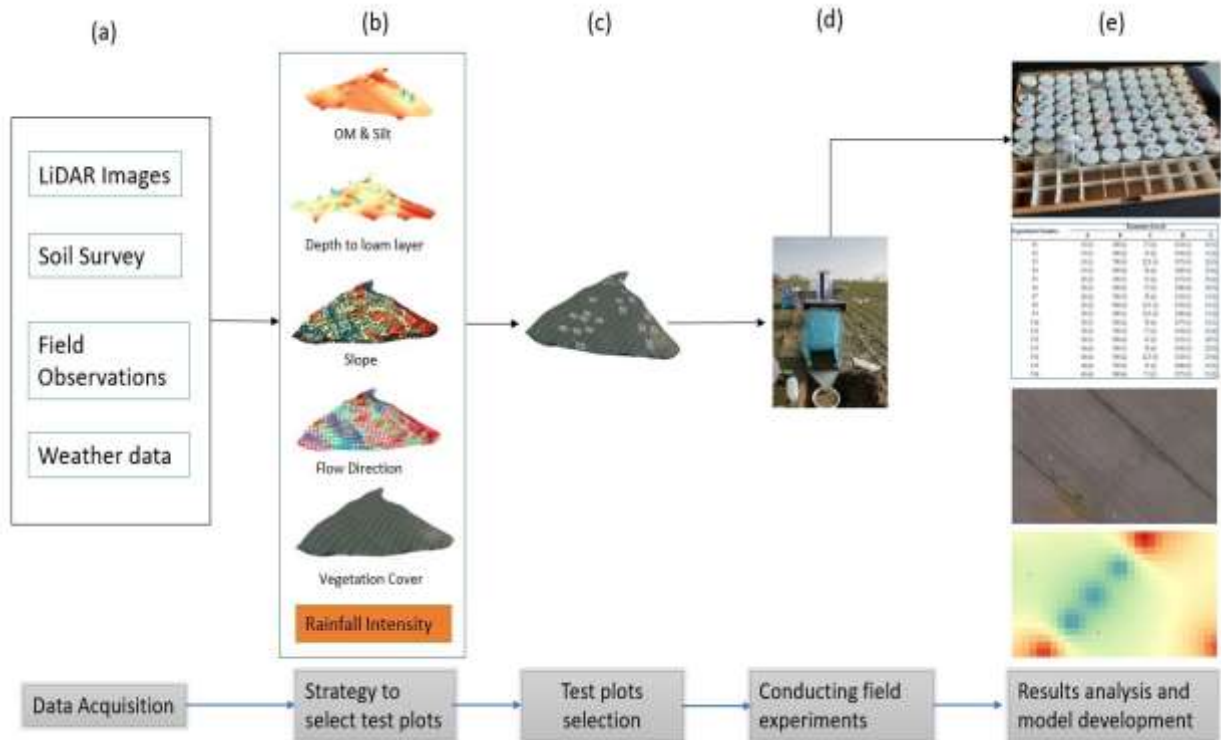
**Table 2: Taguchi fractional factorial design L16 (4<sup>5</sup>) used in this study**

Factors \ Plot ID	Combination of levels					SiltOM (%)	Vegetation cover (%)	Slope steepness (%)	Rainfall intensity (mm min <sup>-1</sup> )	Depth to loamy layer (cm)
	1	2	3	4	5					
<b>1</b>	1	1	1	1	1	>20	1-5	<1	<2.5	<40
<b>2</b>	1	2	2	2	2	>20	0	1-3	2.7-3.3	40-55
<b>3</b>	1	3	3	3	3	>20	10-15	3-5	3.4-4	55-70
<b>4</b>	1	4	4	4	4	>20	>15	>5	>4	>70
<b>5</b>	2	1	2	3	4	18-20	1-5	1-3	3.4-4	>70
<b>6</b>	2	2	1	4	3	18-20	0	<1	>4	55-70
<b>7</b>	2	3	4	1	2	18-20	10-15	>5	<2.5	40-55
<b>8</b>	2	4	3	2	1	18-20	>15	3-5	2.7-3.3	<40
<b>9</b>	3	1	3	4	2	16-18	1-5	3-5	>4	40-55
<b>10</b>	3	2	4	3	1	16-18	0	>5	3.4-4	<40
<b>11</b>	3	3	1	2	4	16-18	10-15	<1	2.7-3.3	>70
<b>12</b>	3	4	2	1	3	16-18	>15	1-3	<2.5	55-70
<b>13</b>	4	1	4	2	3	<16	1-5	>5	2.7-3.3	55-70
<b>14</b>	4	2	3	1	4	<16	0	3-5	<2.5	>70
<b>15</b>	4	3	2	4	1	<16	10-15	1-3	>4	<40
<b>16</b>	4	4	1	3	2	<16	>15	<1	3.4-4	40-55

244

## 245 2.4. Plot selection

246 To select plot locations for experimental runs covering each of the 16 factorial combinations (Table  
247 2), field maps on the depth to a loamy layer, slope inclination, and the sum of silt and OM were  
248 prepared, using SAGA within QGIS 3.16 (Fig. 3). Data on the depth to a loamy layer was derived  
249 from field surveys. Point data were spatially interpolated using ordinary kriging in SAGA. The  
250 topography was derived from 2008 LiDAR imagery (<https://geobroker.geobasis-bb.de>).  
251 Subsequently, map overlays were used to identify 16 plot locations. The 16 locations were  
252 considered to be well distributed in the research site (Fig. 2). At each location, rainfall simulator  
253 experiments were carried out at the respective intensity levels with 4 repetitions. To integrate the  
254 factors “vegetation cover”, simulations were performed on multiple dates with vegetation cover  
255 ranging from 0% (seedbed preparation), over 5% (cultivation) and 10% (crop emergence, DAS:  
256 20) to >15% (leaf development stage 3, DAS: 204) (Table 3).



257

258 **Fig. 3. Schematic diagram of the workflow for the rainfall simulation experiment: (a)**  
 259 **Preprocessing of soil samples and remote sensing data (b) Preparing within-field factor levels**  
 260 **for the Taguchi design (c) Selecting the locations of experimental plots (d) collecting**  
 261 **sediments and runoff (e) Filtering and weighing sediment samples, runoff and CN**  
 262 **concentration in sediments**

263

264 2.5. Rainfall simulator

265 In this study, in order to generate targeted levels of rainfall intensity (Table 2), the portable non-  
 266 pressurized rainfall simulator (Kamphorst, 1987) was used (Fig. 3d). The simulator was produced  
 267 by Eijkelkamp (Eijkelkamp Agrisearch Equipment, Netherlands) and the design is owned by  
 268 Wageningen University Research Centre. The ground coverage area is 0.0625 m<sup>2</sup> enclosed from  
 269 three sides with stainless steel frame. The basic unit of the simulator consists of two Plexiglas  
 270 containers connected with the frame. The upper container has a calibrated cylindrical reservoir  
 271 having a capacity of 2300 ml. The lower container has 49 capillaries with a diameter of 0.6 mm.  
 272 The basic unit is supported with four adjustable legs, 0.4 m average in height, on various slopes.  
 273 Rainfall intensity is controlled by varying the atmospheric pressure inside the basic unit through  
 274 an adjustable aeration pipe attached to the upper container. Fig. 3d illustrates the operation of the  
 275 rainfall simulator in the field. Before the beginning of the experiments, the rainfall simulator was

276 calibrated in order to generate the four different rainfall intensities (Table 2) (Kamphorst, 1987;  
277 “Rainfall simulator - Field measurement equipment | Eijkelkamp,” 2018). Each experiment was  
278 carried out for the duration of 8 minutes keeping in view the storage capacity of the reservoir and  
279 rainfall intensity levels. However, for the rainfall simulator, it is recommended to use it at the  
280 wettest season i.e., soil moisture content near to field capacity, when the soil surface is most  
281 vulnerable to erosion. For that purpose, a pre-wetting of the plot was carried out in the dry season.  
282 The water for pre-wetting is carefully applied through a plastic container with a perforated lid on  
283 it to avoid splash and runoff.

## 284 2.6. Sample preparation

285 The runoff from each plot and repetition and the corresponding sediment yields were collected in  
286 a 2L plastic bucket installed at the downslope end of the stainless steel frame of the simulator. The  
287 samples were thoroughly mixed by stirring before transferring them into plastic bottles. The  
288 volume of samples (runoff + sediment) was determined using glass flasks in the laboratory  
289 followed by wet sieving through a sieve with a mesh size of 2 mm. The samples were then placed  
290 in the oven at 60 °C for drying the dried samples and were later weighted to determine the sediment  
291 yield. There were no stones > 2 mm collected in any of the samples. A pycnometer with distilled  
292 water was used to determine the volume of sediments collected from each experimental plot  
293 (Benjeddou et al., 2017; Heiskanen, 2008). Surface runoff volume was calculated by subtracting  
294 the sediment volume from the total sample volume collected in the field. The sediment samples  
295 were then dried at 60 °C till samples were fully dried to prepare them for carbon and nitrogen (CN)  
296 analysis. The dried samples were transferred then into separate glass scintillation vials and analyzed  
297 for CN content by instantaneous oxidation of the sample via combustion with oxygen at an  
298 approximate temperature of 1020° C using an Elemental Analyzer Euro EA 3000 (EuroVector -  
299 RK Tech Ltd., Pavia)

## 300 2.7. Statistical analysis

301 In Minitab 17.0 software tool, signal-to-noise ratio analyses (SN) were used for the evaluation of  
302 experiment results (Chou et al., 2010; Sivaiah and Chakradhar, 2019). Three types of SN ratios are  
303 used (1) Nominal is better, (2) Higher is better, (3) Lower is better. Because the objective of this  
304 study is to identify the areas with the highest risk of erosion, “the higher the better (HB)” approach  
305 was used. The following equation was used to calculate the SN-ratio:

306 
$$\frac{S}{N_s} = -10 * \log \left( \frac{1}{n} \sum \frac{1}{y^2} \right) \quad (1)$$

307 where,  $n$  represents the number of repetitions at each rainfall simulation plot, and  $y$  represents the  
 308 studied variable. Here,  $y$  is sediment yield, runoff, nitrogen, or carbon content in the sediments  
 309 from each experimental plot.

310 The statistical approach of analysis of mean (ANOM) was used to derive optimal conditions (Parr  
 311 and Taguchi, 1989). ANOM is a graphical method for multiple group comparisons with an overall  
 312 mean (“grand mean”). The mean  $\frac{S}{N_s}$  ratio of each factor  $I$  at a specific level  $i$  (Eqn. 2) was  
 313 determined using the following equation:

314 
$$M_{Factor}^{Level} = \frac{1}{n_{ii}} \sum_{j=1}^{n_{ii}} \left[ \left( \frac{S}{N_s} \right)_{Factor = I}^{level = i} \right]_j \quad (2)$$

315 In equation (2),  $n_{ii}$  is the number of occurrences of factor  $I$  in level  $i$ .  $\frac{S}{N_s}$  response figures and tables  
 316 were obtained, and optimum conditions were established for each concerning output. J?

317 In addition, an analysis of variance (ANOVA) was used to investigate the influence of individual  
 318 factors on sediment yield, runoff, and CN content (Cox et al., 2008). The percentage contribution  
 319 of each experimental factor to the four output variables was estimated using the following equation:

320 
$$\rho_F = \frac{SS_F - (DOF_F V_{ER})}{SS_T} \times 100 \quad (3)$$

321 Where  $V_{ER}$  is the variance of error,  $SS_F$  is the factorial sum of squares, and  $DOF_F$  represents a  
 322 degree of freedom obtained by subtracting one from the number of levels of each factor ( $L$ ). The  
 323 total sum of squares,  $SS_T$ , was calculated using the following equation:

324 
$$SS_T = \sum_{j=1}^m \left( \sum_{i=1}^L Y_i^2 \right)_j - mn \left( \bar{Y}_t \right)^2 \quad (4)$$

325  $Y_t$  is obtained as:

326 
$$\bar{Y}_t = \sum_{j=1}^m \left( \sum_{i=1}^L Y_i \right)_j / mn \quad (5)$$

327 Where,  $m$  represents the number of experimental plots covered in this study, and  $n$  represents the  
 328 number of repetitions under the same experimental plot. The factorial sum of squares,  $SS_F$ , is given  
 329 by:

$$330 \quad SS_F = \frac{mn}{L} \sum_{k=1}^L (\bar{Y}_K^F - \bar{Y}_t) \quad (6)$$

331  $\bar{Y}_K^F$  is the average value of the measurement results of a certain factor in the  $k$ th level. Furthermore,  
 332 the variance of error,  $V_{ER}$  was given by:

$$333 \quad V_{ER} = \frac{SS_T - (\sum_{F=A}^D SS_F)}{m(n-1)} \quad (7)$$

334

### 335 **3. Results and discussion**

#### 336 **3.1. Sediment yield**

337 The variation of sediment yield depending on the five factors and their levels is shown in Fig 4A  
 338 and 5A respectively. The average amount of sediment yield across replicates varies from  $499.2 \pm$   
 339  $20.6$  to  $60.5 \pm 17.3 \text{ g m}^{-2}$ . Plot-based rainfall simulation data show pronounced relative differences  
 340 in sediment yield among different combinations of factors and their respective levels (Fig. 4A).  
 341 Experimental plot B10 (0 % vegetation cover, a rainfall intensity of  $3.4\text{-}4 \text{ mm min}^{-1}$ , the slope of 4  
 342 %, SiltOM 16-18% of and DLL of < 40cm) shows the highest sediment mass with  $499.2 \text{ g m}^{-2}$ ,  
 343 indicating the highest erosion levels under these conditions. The lowest sediment mass ( $60.5 \text{ g m}^{-2}$ )  
 344 was obtained at plot L12 (vegetation cover was >15 %, rainfall intensity <  $2.5 \text{ mm min}^{-1}$ , and  
 345 slope between 1 and 3 %). Fig 5 shows the means of sediment yield for each factor and each level  
 346 and compares them to the overall factor mean (grand mean, dashed line) (ANOM). These graphs  
 347 show that the amount of sediment increases with an increase in rainfall intensity (Fig. 5A). The  
 348 minimum rainfall intensity needed to initiate soil erosion, in this study, was  $2.5 \text{ mm min}^{-1}$ . At lower  
 349 rainfall intensities, the infiltration rate is higher in the beginning. The potential kinetic energy of  
 350 raindrops is small and the splash effect is weak and so is the sediment yield. In addition, runoff  
 351 volume is relatively small under lower rainfall intensities (Mohamadi and Kaviani, 2015). The  
 352 relationship between rainfall intensity and sediment yield varied across intensity levels in a  
 353 systematic way (Fig. 5A). The sediment yield increased to  $204.9 \text{ g m}^{-2}$  when the RI increased to  
 354 level 2, which was  $73.5 \text{ g m}^{-2}$  higher than at RI level 1. The increment was  $253.3 \text{ g m}^{-2}$  and  $310.7$   
 355  $\text{g m}^{-2}$  with RI levels 3 and 4 respectively, where sediment yields were respectively 1.9 and 2.4  
 356 times higher than at RI level 1 (Fig. 5A). This result may indicate that at the plot scale, soil loss

357 would linearly increase up to a threshold of rainfall intensity, beyond which soil loss would increase  
358 non-linearly. Similarly, (Kandel et al., 2004) found a non-linear relationship between high-intensity  
359 rainfall and soil erosion processes. Therefore, it can be suggested that high rainfall intensities  
360 resulted in greater soil losses. This is also confirmed by other studies where high intensity rainfall  
361 events increased sediment yield (Jebari et al., 2008; Sukartaatmadja et al., 2003; Ziadat and  
362 Taimeh, 2013a) and sediment transport.

363 Soil detachment and runoff significantly increased with rainfall intensity for both uncultivated and  
364 cultivated lands (Ziadat and Taimeh, 2013b) but the level of vegetation cover has a significant  
365 effect on the soil detachment. As for plot B10, the same rainfall intensity of 3.4–4 mm min<sup>-1</sup> was  
366 applied to plots E3, C5, and L16 producing 188.1 g m<sup>-2</sup>, 207 g m<sup>-2</sup>, and 199 g m<sup>-2</sup> average sediment  
367 yield respectively (Fig. 4). However, in plot B10 the sediment yield was 499.2 g m<sup>-2</sup>. Among the  
368 rates of sediment yield for four vegetation covers analyzed in this study, vegetation cover level 4  
369 was found most beneficial for preventing soil losses. The eroded sediment yield was below 149 g  
370 m<sup>-2</sup> when the vegetation cover was more than 15 % (level 4). The sediment yield generally tended  
371 to decrease with an increase in vegetation cover (Table 3). The highest mean sediment yield  
372 (averaged across all other factors) was observed after seedbed preparation (vegetation cover 0 %)   
373 with 292.16 g m<sup>-2</sup> (Fig. 5A). In this study, increasing vegetation cover dramatically reduces  
374 sediment yield which is in accordance with the results of (Donjadee and Chinnarasri, 2012; Lin et  
375 al., 2018). (Zapata et al., 2021) mentioned that the vegetation cover interception reduces the  
376 diameter of the drops reaching the soil surface and hence reduces the kinetic energy of a raindrop.  
377 (Huang et al., 2012) also described that vegetation cover increases soil surface roughness that acts  
378 as a barrier to impede surface runoff and increases infiltration time. Thus, vegetation cover reduces  
379 the sediment yield by reducing the kinetic energy of raindrops, intercepting rainfall, increasing  
380 surface roughness, and enhancing infiltration times.

381 A positive relationship was further detected between slope and sediment yield. The sediment yield  
382 increased from 162.24 g m<sup>-2</sup> at a slope of 1 % to 297.44 g m<sup>-2</sup> at a slope of 5 % Fig. 5A. Previous  
383 studies also show that the sediment yield increases with increasing slopes. This indicates a strong  
384 positive relationship between slope and sediment yield (Grismer, 2012). Under extreme rainfall  
385 intensities, it has been observed that surface runoff velocity and sediment yield are primarily driven  
386 by slope inclination (Yan et al., 2018). These observations are likely related to higher overland  
387 flow velocities at higher slope gradients (Defersha and Melesse, 2012) resulting in higher sediment

388 yield. A gentle slope is less subject to activation and transportation of eroded sediments.  
389 Additionally, the splashing effect of raindrops generates surface sealing on gentle slopes producing  
390 more surface runoff carrying sediments. Soil particles are detached from the steep slopes where  
391 downward gravity is comparatively large. Therefore, there is a tradeoff between rainfall intensity  
392 and slope gradient. (Wu et al., 2018b) proved that rainfall intensity has more influence than slope  
393 gradient on sediment yield.

394 The surface soil texture also governs the sediment yield under varying rainfall intensity events.  
395 Water availability and water holding capacity are largely dependent on the texture of the soil  
396 profile, especially under rain-fed conditions (Libohova et al. 2018; Wang et al. 2020; Zhou et al.  
397 2020). The decreasing concentration of SiltOM in the surface soil showed an increasing trend in  
398 sediment yield except for level 4 (2.5 %) which produced a mean sediment yield of  $263.52 \text{ g m}^{-2}$   
399 which was slightly lower than at level 3 ( $275.84 \text{ g m}^{-2}$ ). The detachment of soil is mainly affected  
400 by the size and weight of soil particles, organic matter, and the kinetic energy of the raindrops  
401 (Sadeghi et al., 2017). The silt content varies from 10.2 to 19.5 % in the study area. The loose  
402 particles of silt showed a higher tendency to detachment and erosion process. Soil erodibility  
403 increases with increasing silt content (Baruah et al., 2019) but it reduces drastically once the crust  
404 is formed. However, SiltOM explicated the strong negative effects of mean weight diameter on  
405 splash erosion, and the indirect impact of high organic matter ( $> 2\%$ ) on splash erosion by  
406 improving the aggregate stability (Sun et al., 2021). Moreover, With high rainfall intensity and  
407 longer test duration, detaching capacity was achieved faster and a surface seal appeared on the soil  
408 surface (Michel et al., 2014).

### 409 3.2. Surface runoff

410 At different growth stages of the crop, the runoff process at different rainfall intensities, slope  
411 gradients, and soil textures are shown in Fig. 4B. The observed mean runoff volume varies between  
412  $23.5 \pm 1.07$  and  $6.54 \pm 0.62$  mm among the plots. The plots where rainfall intensity level 4 was  
413 applied showed 42.5 % more surface runoff compared to those plots with rainfall intensity level 1.  
414 The increase of runoff in the low rainfall intensities was gentle and later it tend to be large. In  
415 general, for the highest rainfall intensity, the recorded runoff depth varied from 23 mm to 17.2 mm.  
416 On the other hand, for the events with the lowest rainfall intensity, the recorded runoff depth varied  
417 from 10.4 to 6.8 mm. According to the comparison with local meteorological data from the closest

418 weather station, these two classified intensities can be termed as moderate rainfall intensity events  
419 and high-intensity storm events respectively. Both of which can produce surface runoff on local  
420 slopes in the study area. In our simulation experiments, the rainfall intensity shows a positive  
421 relationship with the depth of surface runoff under all vegetation covers. The high rainfall intensity  
422 occurring in short duration results in a higher runoff depth (Krisnayanti et al., 2021). The diameter  
423 and threshold raindrop velocity tends to increase with higher intensity rainfall. This event is  
424 particularly noticeable when the rainfall intensity is at level 4. Heavy raindrops provide more  
425 kinetic energy which changes the surface roughness producing pores blockage and soil crusts,  
426 which yield higher surface runoff (Lu et al., 2016).

427 The increasing surface runoff depth is positively related to rainfall intensity at the same slope  
428 inclination level and displayed order of  $2.5 \text{ mm min}^{-1} < 2.7\text{-}3.3 \text{ mm min}^{-1} < 3.4\text{-}4 \text{ mm min}^{-1} < 4 \text{ mm}$   
429  $\text{min}^{-1}$  (Fig. 5B). However, the analyses of the relationship between slope gradient and runoff show  
430 increasing surface runoff were observed when the slope increased from 1–3 % (level 2) to >5%  
431 (level4) with runoff depth of 10.66 mm and 15.93 mm, respectively. However, it was decreased  
432 from 13.573 mm to 10.66 mm despite an increasing slope gradient from <1 % (level 1) to 3 %  
433 (level2) and also dropped to 15.08 mm when the slope was >5 % (level 4). The main reason is that  
434 observations at slope levels 1 and 2 are performed for soil class 1 and class 2, with high and  
435 moderate permeability, respectively (Fig. 2A). Previous studies also indicate that surface flow  
436 decreases with increasing slope gradient as the rain-bearing area becomes small as at smaller slope  
437 gradient the infiltration time is longer at the beginning with high permeable soil conditions (Deng  
438 et al., 2019; Wu et al., 2018a). Also, other studies show that surface runoff increases and tend to  
439 stabilize with the further increase of the slope gradient (Zhong and Zhang, 2011) but some studies  
440 also show that runoff increases first and then start decreasing with increasing slope gradient  
441 (Jourgholami et al., 2021; Li et al., 2020; Li and Yu, 2012). The present study shows similar results.  
442 Guo et al., (2018) showed that runoff depth is directly related to rainfall intensity and in a negative  
443 relationship with slope gradient. Infiltration rates decrease as slope increases from  $6^\circ$  to  $35^\circ$  and,  
444 thus, runoff depth increases to a certain extent until a critical slope gradient of  $11^\circ$  is reached at  
445 which infiltration rate trend starts changing (Liu et al., 2015). With further increments in slope, the  
446 runoff depth gradually decreases (Jourgholami et al., 2021; Nassif and Wilson, 1975). The rainfall  
447 intensity has more impact on runoff than slope gradient in this study which is in line with the work

448 by (Wu et al., 2018b). Since the slope gradients at our research site are well below 10 degrees the  
449 stronger impact of rainfall intensities agrees with other studies (Liu et al., 2015)

450 In this study, vegetation cover had a positive relationship with runoff depth. Fig. 5B shows that  
451 from level 1 (1-5 %) to level 2 (0 %) of vegetation cover there is an abrupt increase in surface  
452 runoff as on bare soil there are no interception losses. Then the runoff depth increases with  
453 increasing vegetation cover from level 3 (10-15 %) to level 4 (>15 %). The runoff depth was in the  
454 order of level 4 > level 2 > level 3 > level 1 of vegetation cover for both high and low rainfall  
455 intensity and all slope gradients. However, many studies show that runoff decreases with increasing  
456 vegetation cover due to higher canopy interception and rain redistribution reduces energy and  
457 runoff depth (He et al., 2020; Loch, 2000; Meng et al., 2007; Tong Li et al., 2020). The reason for  
458 high runoff depth at high vegetation cover can be hydrophobic repellency (De Jonge et al., 2007;  
459 Hermansen et al., 2019; Knadel et al., 2016) of the surface soil, as higher vegetation cover extracts  
460 more soil water. In fact, low soil moisture conditions under higher vegetation cover as noted during  
461 the field experiments. Many studies have reported that surface runoff depth increases under dry  
462 conditions such as drought periods (Burch et al., 1989; Buttle and Turcotte, 1999; Gomi et al.,  
463 2008; Sosa-Pérez and MacDonald, 2017). These studies suggested that the generation of  
464 hydrophobic soil surface conditions was one of the main reasons for this phenomenon under dry  
465 conditions. (Burch et al., 1989) for example, found that runoff depth increases from 5 % to 15 %  
466 due to the hydrophobic conditions after drought or dry summer. These previous studies suggest  
467 that because of drought development water repellent soil surface conditions produce more surface  
468 runoff regardless of high vegetation cover. The size of the plot can also have a significant impact  
469 on the runoff depth. Results obtained by Smets et al. (2008) indicate that there is significant  
470 variation in the effectiveness of vegetation cover on runoff if the plot is less than 11m long. Plot  
471 scale significantly affects the influence of surface roughness and vegetation cover on sediment  
472 yield and runoff depth (Jourgholami and Labelle, 2020).

473 The runoff depth changed with changing silt and organic material content among plots and results  
474 suggest that effects are significant ( $p < 0.027$ ). The results agree with Vaezi et al. (2010), who also  
475 observed that runoff significantly correlated with silt ( $p < 0.001$ ) and organic material ( $p < 0.05$ ).  
476 Organic material positively affects the soil permeability, hence reducing the surface runoff depth  
477 (Sepaskhah and Bazrafshan-Jahromi, 2006). A similar pattern was observed for levels 1, 2, and 4  
478 of this factor with the runoff averaging 14.05 mm, 13.82 mm, and 12.50 mm, respectively. Slightly

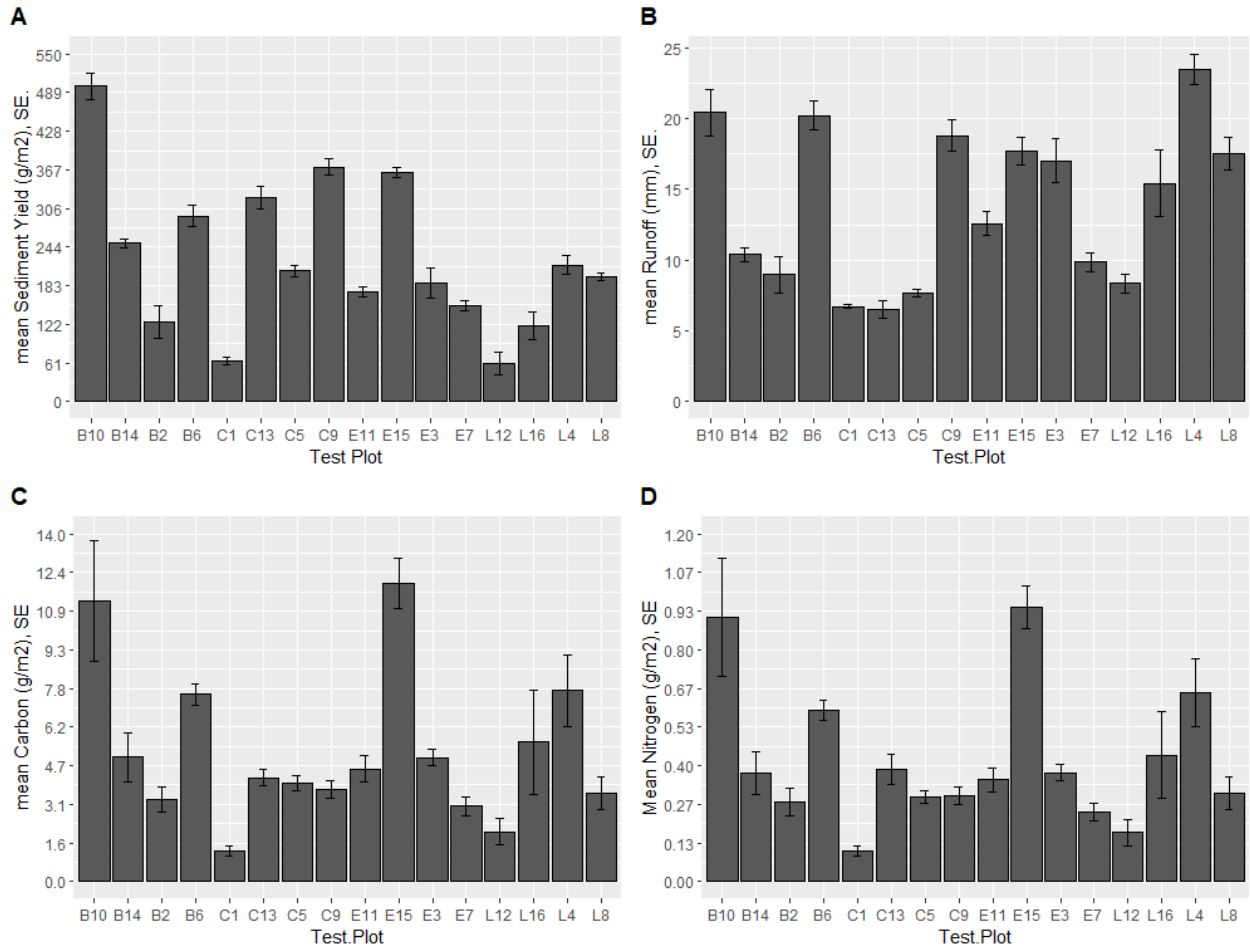
479 increasing runoff depth at level 3 was observed. Results agree with studies indicating that the  
480 primary factors affecting surface runoff during rainfall simulation experiments are current soil  
481 moisture levels, soil texture, slope, and rainfall intensity (Wang et al., 2016; Ziadat and Taimeh,  
482 2013b). The highest runoff was recorded with 23 mm at plot B10 where SiltOM was at level 3 (Fig.  
483 4) (Table. 4) and depth to loamy layer < 40 cm (Fig. 2). Later the runoff depth tends to decrease  
484 to 12.4 mm as SiltOM percentage increases in the field to level 4. A general trend in this study  
485 depicts that with increasing SiltOM content there is a decrease in surface runoff depth with a slight  
486 difference at level 3 The depth to a loamy layer (DLL) may act contrary to the effect of the silt  
487 content on runoff depth. A thicker sandy topsoil (i.e. deeper depth to loamy layer) may positively  
488 affect the soil permeability increasing the infiltration and consequently reducing the surface runoff  
489 depth. Thus, spatial variation in these soil properties in the study area noticeably influences the  
490 runoff generation in the test plots. This has been also proved in previous studies (Brakensiek and  
491 Rawls, 1994; Hrabovský et al., 2020; Meena et al., 2020) mentioning that spatial variability of  
492 infiltration capacity is related to the spatial variability of topsoil characteristics that consequently  
493 affect the runoff generation.

### 494 3.3. Carbon and Nitrogen concentration in sediment yield

495 Soil carbon and nitrogen concentration redistribution is strongly governed by the amount of  
496 detached sediment within cultivated lands and it is generally accepted that C and N are  
497 preferentially transported during soil erosion (Holz and Augustin, 2021). The average values of  
498 carbon and nitrogen losses under each level of vegetation cover, slope, and rainfall intensities are  
499 presented in Fig. 4C & 4D respectively. Nitrogen and carbon contents of observed sediment yields  
500 are highly correlated and vary among experimental plots (Fig 4. C & D). Total C and N losses  
501 ranged between  $12 \pm 1.02$  to  $3.29 \pm 0.496$  g m<sup>-2</sup> and  $0.948 \pm 0.073$  to  $0.106 \pm 0.016$  g m<sup>-2</sup> respectively  
502 with moderate to high standard deviation, depending on RI, vegetation cover percentage, and  
503 SiltOM content (Fig. 4. C & D). As reported for the soil loss, C and N losses on the plots were  
504 positively related to the rainfall intensity ranging between 2.8 to 7.7 g m<sup>-2</sup> and 0.2 to 0.4 g m<sup>-2</sup> (Fig.  
505 4).

506 In Figure 5C and 5D, it is obvious that the highest nutrient losses were found at vegetation cover  
507 more than 0 % despite other land covers percentages contributing less to the nutrient losses (Fig.  
508 5. C & D). However, C and N losses were higher in at a vegetation cover of 15 % and in barren

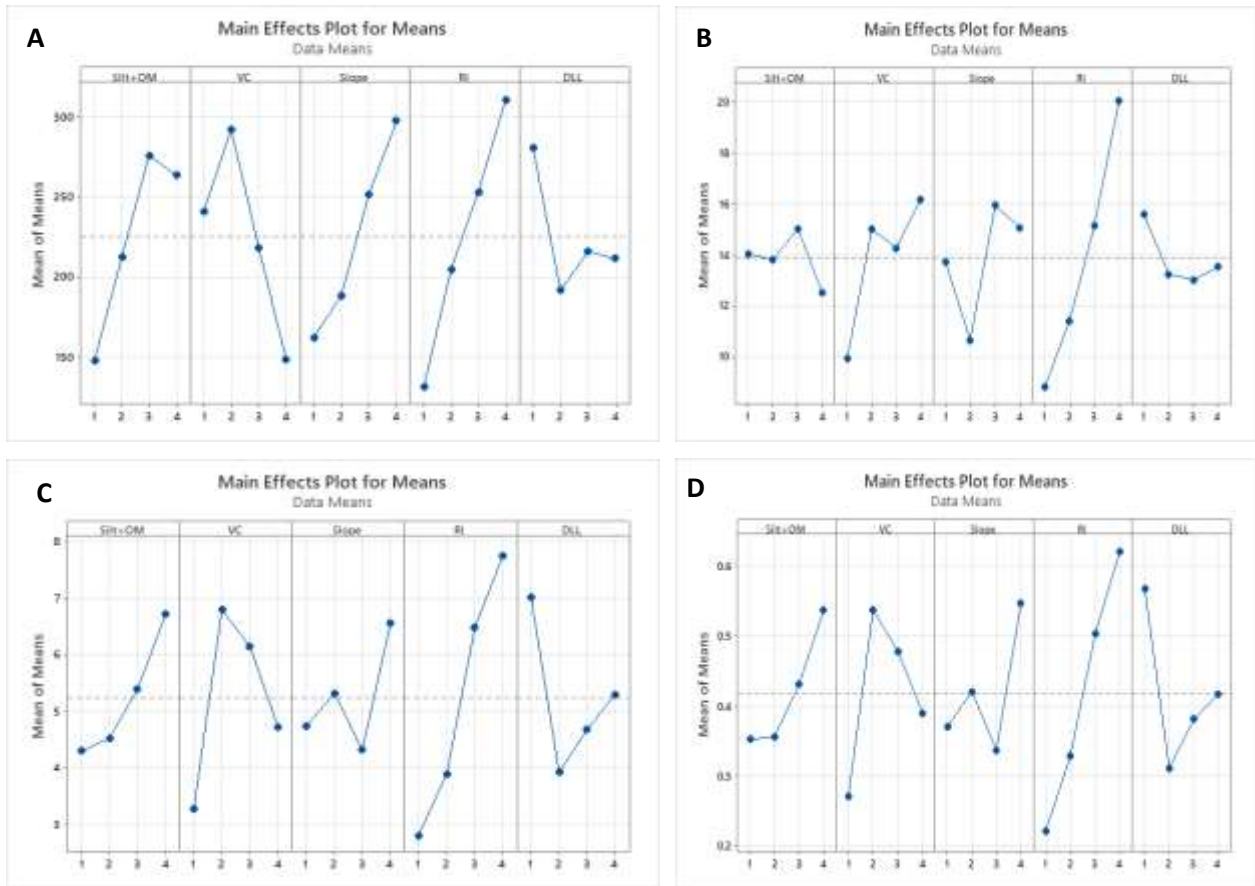
509 land when the soil was subjected to rainfall intensity level 4 ( $4 \text{ mm min}^{-1}$ ) (Fig. 4. C & D). This  
510 behavior is related to the absence of topsoil protective cover that reduces the impact of raindrops  
511 and detachment of soil particles (Nunes et al., 2011). The highest C loss was found under RI of  $>$   
512  $4 \text{ mm min}^{-1}$  with values ranging between  $12 \pm 1.02 \text{ g m}^{-2}$  and  $7.68 \pm 1.12 \text{ g m}^{-2}$  after 8 min rainfall,  
513 respectively for vegetation cover levels 4 and 3 (Fig. 5C). Regarding N losses, the highest losses  
514 were recorded in the plots with the highest C losses. The smallest C and N loss was observed as  
515  $2.8$  and  $0.2 \text{ g m}^{-2}$  respectively at low rainfall intensities when detachment forces were small (Fig.  
516 5. C & D). The experiments carried out in this study confirm the soil susceptibility to loose nutrients  
517 under specific vegetation cover, even at a low rainfall intensity level ( $< 2.5 \text{ mm min}^{-1}$ ). All the  
518 study plots have varying silt and organic matter contents, which made soils to lose nutrients  
519 defining crusting indexes (Awadhwai and Thierstein, 1985). The different values of runoff induce  
520 differences in sediment yield and transport of nutrients. Higher rainfall intensities produce higher  
521 runoff depth. It could be confirmed that nutrient losses increase exponentially with higher rainfall  
522 intensities. The analysis of slope gradient effect on nutrient loss, where higher soil losses occur,  
523 shows that soil sealing can be the main factor that limits runoff as it does not increase significantly  
524 with increasing slope (Fig. 5B) (Ramos et al., 2019). However, as sediment yields are increasing  
525 with an increasing slope so do the C and N losses captured in the collected sediments except at  
526 slope level 3 where C and N losses are reduced as slope increases from level 2 to level 3. The  
527 reason is probably that the plots with slope level 3 lie in soil class 3 with throughout sandy texture  
528 and lower C and N concentrations in the topsoil (Yost and Hartemink, 2019). The results suggest  
529 that a permanent vegetation cover is essential to reduce C and N losses.



530  
 531 **Fig. 4: Mean temporal variations and standard error (SE) in sediment yield, runoff, carbon,**  
 532 **and nitrogen in relation to heterogeneous field conditions**

533  
 534 **Table 3: Mean sediment yield observed under changing soil surface conditions (vegetation**  
 535 **cover factor levels)**

Field condition	Vegetation cover	Mean sediment yield	Standard error
	%		
<b>Cultivation</b>	5	241	31.1
<b>Seedbed reparation</b>	0	292	35.8
<b>Emergence stage</b>	10	219	22.5
<b>Leaf development (3 Leaves unfold)</b>	15	149	17.7



538

539 **Fig. 5: Analysis of means (ANOM) for A: Sediment yield ( $\text{g m}^{-2}$ ), B: Runoff (mm), C: Carbon**  
 540 **( $\text{g m}^{-2}$ ), D: Nitrogen content ( $\text{g m}^{-2}$ ). Mean values for each level of each factor (blue dots) and**  
 541 **the overall mean of each factor (dashed green line) are shown.**

542 3.4. Optimal conditions for maximum sediment yield, surface runoff, Nitrogen, and Carbon  
 543 content

544 The obtained S/N ratio responses for sediment yield, surface runoff, carbon, and nitrogen content  
 545 are shown in Table 4 and Table 5. A Higher S/N ratio implies low variations between the desired  
 546 output and the measured output. The maximum S/N ratio values among the 16 experiments,  
 547 indicated in table 4 were 53.97 for sediment yield and 26.21 for runoff, 21.59 and -0.81 for C and  
 548 N losses respectively in the test plot 10 with factor combination of SiltOM<sub>3</sub>-VC<sub>2</sub>-SS<sub>4</sub>-RI<sub>3</sub>-DLL<sub>1</sub>  
 549 (Table 4). Inserting these values from table 4 into Eqn. 2 resulted in mean values of S/N ratios for  
 550 each factor level. The maximum values of means of the S/N ratio were then identified. The bold  
 551 values in Table 5 show the factor level with the highest S/N ratio for each factor and output variable  
 552 (sediment yield, runoff, C and N losses). The highest mean S/N ratio for sediment yield was

553 obtained at factor level 4 for SiltOM, SS, and RI, at level 2 for VC, and level 1 for DLL (Table 5).  
554 Thus, we can predict that the highest sediment yield should be obtained with the factor level  
555 combination SiltOM<sub>4</sub>-VC<sub>2</sub>-SS<sub>4</sub>-RI<sub>4</sub>-DLL<sub>1</sub> (Table 5). On the other hand, the lowest sediment yield  
556 should be obtained with the factor combination SiltOM<sub>1</sub>-VC<sub>4</sub>-SS<sub>1</sub>-RI<sub>1</sub>-DLL<sub>2</sub>. The estimated  
557 optimum factor level combination for obtaining the highest surface runoff was found to be  
558 SiltOM<sub>3</sub>-VC<sub>4</sub>-SS<sub>3</sub>-RI<sub>4</sub>-DLL<sub>1</sub> (Table 5). The highest rainfall intensity (>4 mm min<sup>-1</sup>) led to the  
559 highest volumes of runoff, followed by the factor vegetation cover (maximum values at Level 4)  
560 (Table 5). Earlier studies showed that surface runoff depth is sensitive to the plot size and type of  
561 vegetation (Herweg and Ludi, 1999; Kort et al., 1998; Zuazo and Pleguezuelo, 2008). The optimum  
562 condition for maximum C and N losses were found to be SiltOM<sub>4</sub>-VC<sub>2</sub>-SS<sub>4</sub>-RI<sub>4</sub>-DLL<sub>1</sub> and SiltOM<sub>4</sub>-  
563 VC<sub>2</sub>-SS<sub>4</sub>-RI<sub>4</sub>-DLL<sub>1</sub> respectively (Table 5). The results indicate that rainfall intensity was the main  
564 factor that most influenced the sediment yield, runoff, C and N losses in the study area followed  
565 by vegetation cover and then slope steepness.

566  
567  
568  
569  
570  
571  
572  
573  
574  
575  
576  
577  
578  
579  
580  
581

582 **Table 4: The S/N ratio of each experiment resulting from a different combination of factors**  
 583 **and levels.**

Factors/ Plot	Combination of levels					Silt OM (%)	vegetation cover (%)	Slope steepness (%)	Rainfall intensity (mm min <sup>-1</sup> )	Depth to loamy layer (cm)	S/N			
	Silt OM	VC	SS	RI	DLL						Sediment yield	Runoff	C	N
1	1	1	1	1	1	>20	1-5	<1	<2.5	<40	36.08	16.53	1.65	-19.47
2	1	2	2	2	2	>20	0	1-3	2.7-3.3	40-55	41.98	19.05	10.35	-11.20
3	1	3	3	3	3	>20	10-15	3-5	3.4-4	55-70	45.47	24.62	13.96	-8.48
4	1	4	4	4	4	>20	>15	>5	>4	>70	46.70	27.42	17.71	-3.72
5	2	1	2	3	4	18-20	1-5	1-3	3.4-4	>70	46.31	17.70	11.96	-10.69
6	2	2	1	4	3	18-20	0	<1	>4	55-70	49.35	26.12	17.55	-4.56
7	2	3	4	1	2	18-20	10-15	>5	<2.5	40-55	43.60	19.87	9.65	-12.44
8	2	4	3	2	1	18-20	>15	3-5	2.7-3.3	<40	45.95	24.87	11.01	-10.35
9	3	1	3	4	2	16-18	1-5	3-5	>4	40-55	51.39	25.48	11.43	-10.58
10	3	2	4	3	1	16-18	0	>5	3.4-4	<40	53.97	26.21	21.59	-0.81
11	3	3	1	2	4	16-18	10-15	<1	2.7-3.3	>70	44.75	21.98	13.13	-9.09
12	3	4	2	1	3	16-18	>15	1-3	<2.5	55-70	35.63	18.42	6.02	-15.45
13	4	1	4	2	3	<16	1-5	>5	2.7-3.3	55-70	50.18	16.31	12.41	-8.20
14	4	2	3	1	4	<16	0	3-5	<2.5	>70	47.97	20.32	13.99	-8.54
15	4	3	2	4	1	<16	10-15	1-3	>4	<40	51.18	24.95	21.05	-0.46
16	4	4	1	3	2	<16	>15	<1	3.4-4	40-55	41.52	23.76	15.01	-7.19

584

585

586

587

588

589

590

591

592

593

594 **Table 5: Mean S/N ratio response table for the investigated experimental factors**

Output Parameter	Experimental factors	Mean S/N ratio				Delta	Rank
		Level 1	Level 2	Level 3	Level 4		
<b>Sediment Yield</b>	Silt+Organic material	42.56	46.30	46.44	<b>47.71</b>	5.15	4
	Vegetation Cover	45.99	<b>48.32</b>	46.25	42.45	5.87	2
	Slope Steepness	42.92	43.78	47.69	<b>48.61</b>	5.69	3
	Rainfall Intensity	40.82	45.71	46.82	<b>49.65</b>	8.83	1
	Depth to Loamy Layer	<b>46.79</b>	44.62	45.16	46.43	2.17	5
<b>Runoff</b>	Silt+ Organic material	21.91	22.14	<b>23.02</b>	21.34	1.69	5
	Vegetation Cover	19.01	22.93	22.86	<b>23.62</b>	4.61	2
	Slope Steepness	22.1	20.03	<b>23.82</b>	22.45	3.79	3
	Rainfall Intensity	18.79	20.56	23.07	<b>25.99</b>	7.21	1
	Depth to Loamy Layer	<b>23.14</b>	22.04	21.37	21.86	1.78	4
<b>Carbon</b>	Silt+ Organic material	10.92	12.54	12.91	<b>15.75</b>	4.83	3
	Vegetation Cover	9.36	<b>15.74</b>	14.58	12.44	6.37	2
	Slope Steepness	11.83	12.48	12.60	<b>15.21</b>	3.37	4
	Rainfall Intensity	7.83	11.73	15.50	<b>17.07</b>	9.24	1
	Depth to Loamy Layer	13.83	11.61	12.49	<b>14.20</b>	2.59	5
<b>Nitrogen</b>	Silt+ Organic material	-10.72	-9.51	-8.98	<b>-6.10</b>	4.61	3
	Vegetation Cover	-12.24	<b>-6.28</b>	-7.62	-9.18	5.95	2
	Slope Steepness	-10.08	-9.45	-9.49	<b>-6.29</b>	3.78	4
	Rainfall Intensity	-13.97	-9.71	-6.79	<b>-4.83</b>	9.14	1
	Depth to Loamy Layer	<b>-7.77</b>	-10.35	-9.17	-8.01	2.58	5

595

596 3.5. Percentage contribution of the experimental factors to sediment yield, runoff, C and N

597 losses

598 ANOVA was used to estimate the contribution of the individual factors to sediment yield, runoff,

599 C and N losses (Table 6). Rainfall intensity contributed most strongly to sediment yield (40.55 %)

600 followed by slope steepness (23.76 %) and vegetation cover (17.73 %). (Peng and Wang, 2012)

601 indicated that soil loss is positively related to rainfall events with high antecedent precipitations.

602 The slope gradient can be more important than vegetation cover because of its relation with the

603 underlying geological formations resulting in varying soil characteristics. In consequence, slope  
604 gradients are related to soil moisture and hence the soil's susceptibility to soil detachment.  
605 Vegetation cover yields higher soil moisture at low to moderate slopes but it falls sharply at steeper  
606 slopes as soil permeability decreases that increases runoff till a threshold slope, moreover, the flow  
607 velocity becomes larger with increasing slope gradient due to increasing shear stress (Defersha and  
608 Melesse, 2012). The impact duration of runoff on steeper slopes becomes smaller and hence it  
609 weakens the protecting effect of surface seal, increasing the impact of rainfall splashing on the soil  
610 surface (Zhao et al., 2015). It produces more detachment of soil particles and transportation.  
611 However, the sum of silt content and organic material only contributes 14.77 % to sediment yield.  
612 (Ziadat and Taimeh, 2013a) showed a significant correlation between the ultimate infiltration rate  
613 and soil properties such as organic matter ( $R = 0.48$ ) and silt content ( $R = 0.72$ ). The low  
614 contribution of silt and organic matter to our results is most likely related to their comparatively  
615 low variation among measurement plots and due to the high content of organic matter that is  
616 varying from 2.3 to 2.4 % among the test plots. The high organic matter improves the aggregate  
617 stability, reduces the bulk density, and increases moisture retention and soil shear strength that  
618 helps in soil stability and resistance against erosion (Ekwue, 1990). Previous studies also concluded  
619 that aggregate stability is closely and negatively related to the soil detachment from field  
620 experiments under rainfall simulators on micro plots (Roth et al., 1987; Van Dijk et al., 1996). The  
621 factor of least importance in our study was the depth to the loamy layer (DLL) (3.17 %). This can  
622 be explained by the fact that the loamy layer with low permeability generally starts at relatively  
623 deep depths (lowest depth approximately 38 cm) and at many locations sand-filled pre-glacial ice  
624 cracks with higher permeability were observed in the loamy layer (Kühn, 2003). Therefore,  
625 differences in permeability and water storage capacity (risk of waterlogged soils) between  
626 experimental plots were probably relatively low. ANOVA results for the nitrogen (N) and carbon  
627 (C) content of sediment yield were similar (Table 6). As for sediment yield, rainfall intensity  
628 contributed most to the overall variation of C and N contents. The respective percentage  
629 contribution of rainfall intensity, vegetation cover, SiltOM content, slope and depth to loamy layer  
630 was 51.70%, 21.50 %, 12.55 %, 9.63 % and 4.62 % respectively for Nitrogen content and 52.31  
631 %, 24.07 %, 12.39 %, 6.81 % and 4.41 % respectively for Carbon content. Runoff was mostly  
632 influenced by rainfall intensity (55.45 %) followed by vegetation cover, slope, depth to loamy  
633 layer, and SiltOM content. The respective contribution was 55.45 %, 24.71 %, 3.18 %, and 2.78 %  
634 (Table 6), agreeing with the findings of (Kirkby et al., 2004). The stronger impact of vegetation

635 cover compared with the slope can be explained by the stronger variability of vegetation cover at  
 636 different soil management stages during the experimental period in the study area. In addition, at  
 637 different slope levels varying soil compositions and moisture content affect the potential of surface  
 638 runoff.

639 **Table 6: Percentage contribution of each factor (ρF %) for the different output parameters**  
 640 **as estimated by ANOVA**

Output Parameters	ρ <sub>F</sub> %				
	SiltOM	Vegetation cover	Slope steepness	Rainfall intensity	Depth to Loamy Layer
<b>Sediment yield</b>	14.77	17.74	23.77	<b>40.56</b>	3.17
<b>Runoff</b>	2.78	24.71	13.88	<b>55.45</b>	3.18
<b>Nitrogen content</b>	12.55	21.50	9.63	<b>51.70</b>	4.62
<b>Carbon content</b>	12.39	24.07	6.81	<b>52.31</b>	4.41

641

642

673 3.6.Linear regression models

674 Linear regression models are used to predict sediment yield, runoff, as well as C and N losses as a  
 675 function of Silt + OM, vegetation cover, slope, rainfall intensity, and depth to the loamy layer. No  
 676 transformation has been performed on the response variables. The estimated regression models are  
 677 shown in the Eqns. (8-11).

678 Sediment yield = -7.2 + 40.9 SiltOM - 35.1 VC + 46.9 Slope + 58.6 RI - 18.4 DLL

679 ( $R^2 = 82.53$ ) (8)

680 Runoff = 0.10 - 0.341 SiltOM + 1.807 VC + 0.933 Slope + 3.743 RI - 0.641 DLL

681 ( $R^2 = 79.66$ ) (9)

682 C = -2.08 + 0.810 SiltOM + 0.371 VC + 0.446 Slope + 1.736 RI - 0.440 DLL

683 ( $R^2 = 60.97$ ) (10)

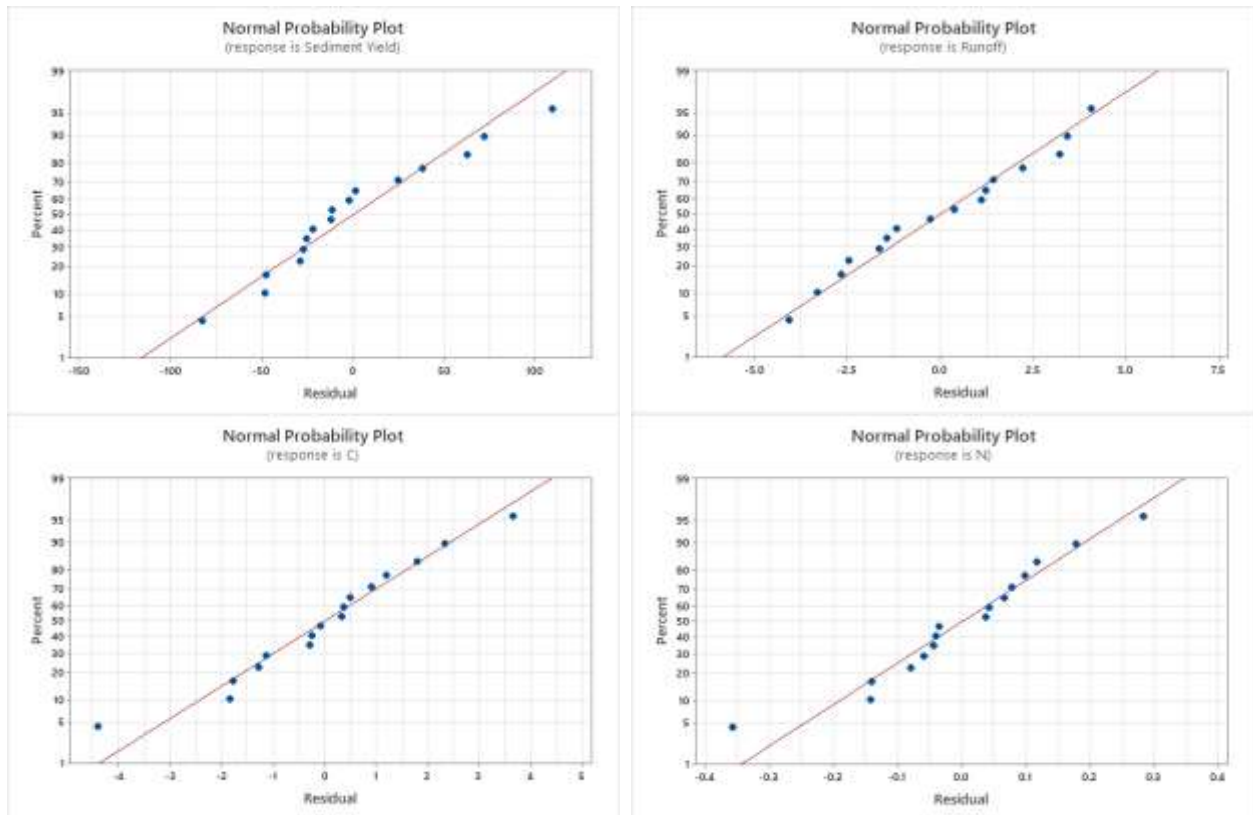
684 N = -0.172 + 0.0629 SiltOM + 0.0299 VC + 0.0445 Slope + 0.1373 RI - 0.0381 DLL

685 ( $R^2 = 62.13$ ) (11)

686 Where sediment yield, runoff depth, C and N are g m<sup>-2</sup>, SiltOM and VC are %.

687

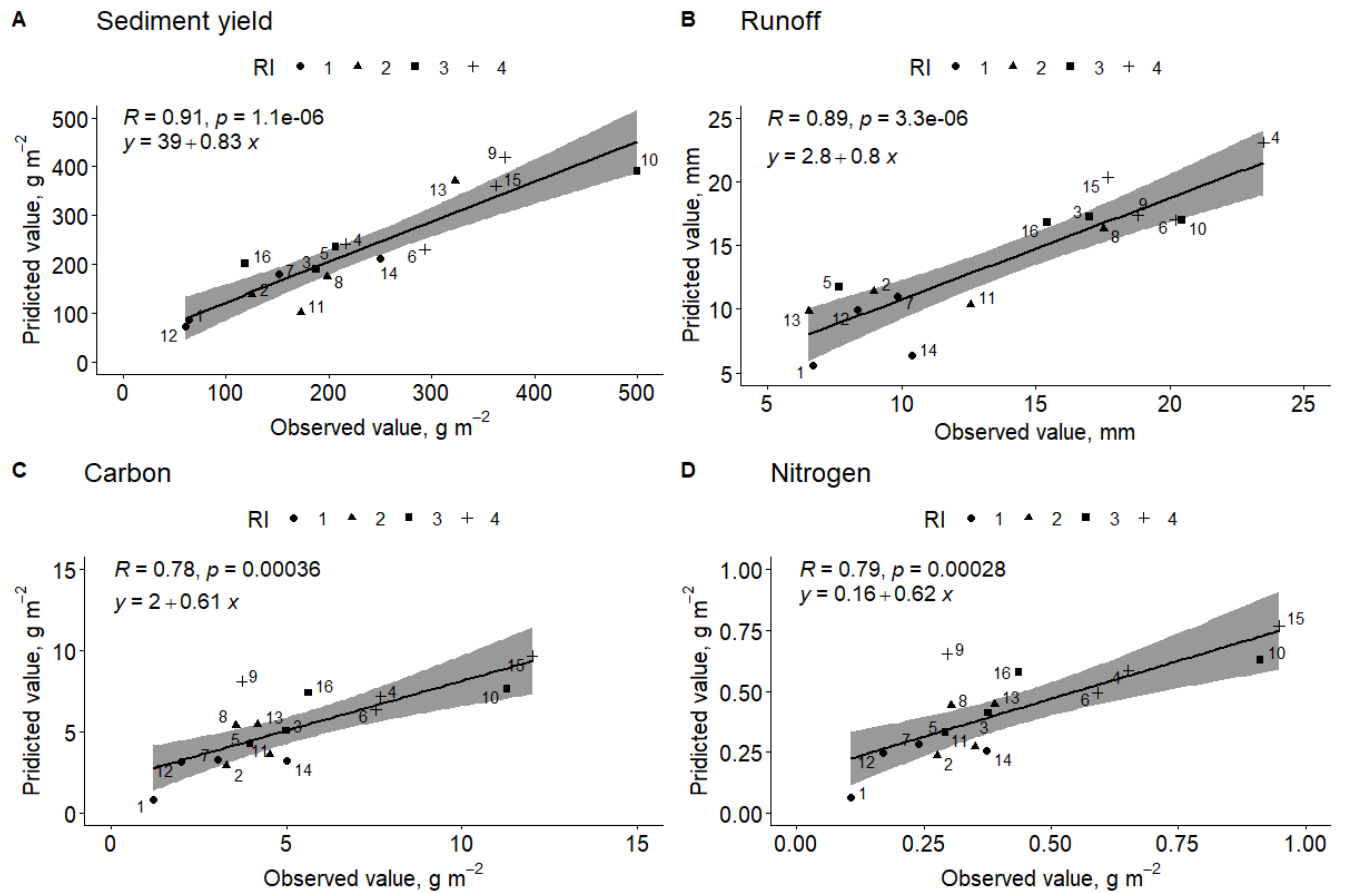
688 The capability of these empirical regression models was checked by using the coefficient of  
689 determination  $R^2$ . Regression models for sediment yield, runoff, carbon, and nitrogen yielded  $R^2$   
690 values of 82.53 %, 79.66 %, 60.97 %, and 62.13 % respectively. Residual plots (Fig. 7 A, B, C &  
691 D) indicate that residuals are independent and normally distributed. Sediment yield is positively  
692 related to SiltOM but runoff depth is negatively related. This indicates that a high amount of SiltOM  
693 would increase the erodibility of the soil but would reduce the runoff rate. This is also evident from  
694 Fig. 5A and B. The sediment yield is more sensitive to SiltOM compared to runoff. Coefficients of  
695 SiltOM for C and N losses show a positive relationship. C was more responsive to SiltOM as  
696 compared to N. It is suggested to have further research to find a threshold point for SiltOM in the  
697 soil to achieve the lowest sediment yield and runoff. Fig. 8 represents the scatter plot of predicted  
698 vs observed values with high  $R^2$ . The shaded band is a pointwise 95 % confidence interval on the  
699 fitted values. These results confirm the ability of the Taguchi method for the prediction of soil  
700 erosion in response to different combinations of factors/levels. The regression equation for  
701 sediment yield was further applied to predict sediment yields across the entire field for identifying  
702 areas within the field that have a higher susceptibility to soil erosion (Fig. 9).



703

704 **Fig. 7: Distribution of residuals of the regression models for sediment yield, runoff, carbon,**  
 705 **and nitrogen**

706



707

708

709 **Fig. 8: Predicted versus observed sediment yield, runoff depth, carbon, and nitrogen losses**

710

711

712

713

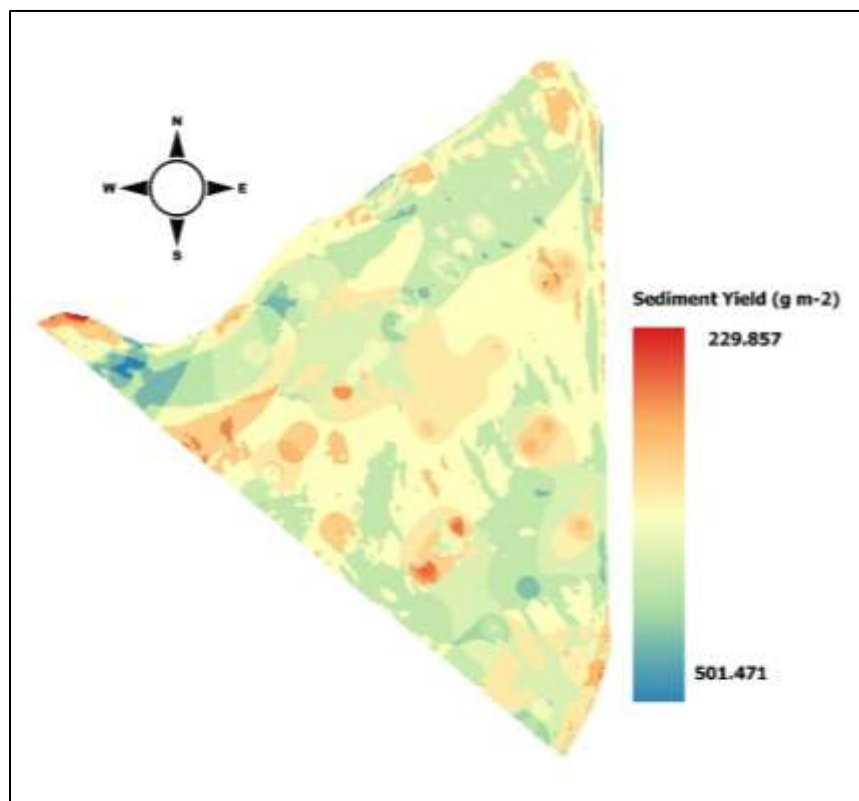
714

715

716

717

718



719

720

721 **Fig. 9: Identification of potential soil erosion risk areas**

722 **4. Conclusion**

723 Different scenarios were tested with 16 effective simulated rainfall events under different rainfall  
 724 intensities, vegetation cover, heterogeneous in-field slope, and soil conditions. The results  
 725 indicated that runoff, soil, and CN losses increase with increasing rainfall intensity. It was observed  
 726 that sediment yield, overland flow, CN content were greatly affected by rainfall intensity having a  
 727 contribution of 40.56 %, 55.45 %, 51.70 %, and 52.31 % respectively among the other factors.  
 728 However, the least contributing factor was depth to loamy layer for all output variables except for  
 729 surface runoff. The results show that the worst conditions among 16 plots were at SiltOM<sub>3</sub>-VC<sub>2</sub>-  
 730 SS<sub>4</sub>-RI<sub>3</sub>-DLL<sub>1</sub> for sediment yield. However, predicted experimental factors for the highest  
 731 sediment yield were found with the factor combination SiltOM<sub>4</sub>-VC<sub>2</sub>-SS<sub>4</sub>-RI<sub>4</sub>-DLL<sub>1</sub> and the lowest  
 732 sediment yield was observed with the factor combination SiltOM<sub>1</sub>-VC<sub>4</sub>-SS<sub>1</sub>-RI<sub>1</sub>-DLL<sub>2</sub>. The  
 733 threshold rainfall intensity for soil erosion was 2.5 mm min<sup>-1</sup>. VC and DLL are inversely correlated  
 734 with sediment yield, while SiltOM, slope, and rainfall intensity are directly correlated.

735 The surface runoff was negatively related to SiltOM and DLL, but the vegetative cover, slope, and  
 736 rainfall intensity positively affect the runoff. Regarding, C and N, except the DLL, other factors  
 737 show a positive correlation. Based on the experimental results, statistical regression models were  
 738 developed, which were applied for identifying the erosion risk areas at the field scale. The applied  
 739 workflow allowed for efficiently predicting soil erosion and identifying areas susceptible to soil  
 740 loss at a high spatial resolution. The study approved the capabilities of Taguchi's fractional

741 factorial design to efficiently analyze the response of soil erosion to dominant driving factors and  
742 detect and quantify in-field heterogeneity of erosion risk areas. The statistical models generated in  
743 this study can be used by environmental agencies and farmers for spatially explicit application of  
744 erosion control measures within fields with high spatial heterogeneity. Further, it is suggested that  
745 combining GIS with such numerical models can give great benefits for water quality control and  
746 soil management on larger scales with intensive spatial heterogeneous field conditions.

#### 747 **CRedit authorship contribution statement**

748 Conceptualization, A.R., T.G., M.H.R., and H.A.; methodology, A.R., M.H.R., T.G., and H.A.; re-  
749 source and data curation, A.R., T.G., and H.A., writing-original draft preparation, A.R.; writing-  
750 review and editing, T.G., M.H.R., H.A., and A.R.; visualization, M.H.R., H.A., and T.G.;  
751 supervision, T.G.; project administration, T.G.; funding acquisition, T.G., H.A.; All authors have  
752 read and agreed to the published version of the manuscript.

#### 753 **Funding**

754 This research was funded by the German Federal Ministry of Education and Research (BMBF)  
755 through the Digital Agriculture Knowledge and Information System (DAKIS) Project, grant  
756 number 031B0729E, and by the Deutsche Forschungsgemeinschaft (DFG, German Research  
757 Foundation) under Germany's Excellence Strategy-EXC 2070-390732324 (PhenoRob). The APC  
758 was funded by the Crop Science Group, University of Bonn, Germany.

#### 759 **Declaration of competing interest**

760 The authors declare that they have no known competing financial interests or personal relationships  
761 that could have appeared to influence the work reported in this paper.

#### 762 **References**

- 763 Aga, A.O., Melesse, A.M., Chane, B., 2020. An alternative empirical model to estimate  
764 watershed sediment yield based on hydrology and geomorphology of the basin in data-  
765 scarce rift VALLEY lake regions, Ethiopia. *Geosci.* 10.  
766 <https://doi.org/10.3390/geosciences10010031>
- 767 Albaladejo Montoro, J., Stocking, M., 1989. Comparative evaluation of two models in predicting  
768 storm soil loss from erosion plots in semi-arid Spain. *Catena* 16, 227–236.  
769 [https://doi.org/10.1016/0341-8162\(89\)90010-6](https://doi.org/10.1016/0341-8162(89)90010-6)
- 770 Anh, P.T.Q., Gomi, T., MacDonald, L.H., Mizugaki, S., Van Khoa, P., Furuichi, T., 2014.  
771 Linkages among land use, macronutrient levels, and soil erosion in northern Vietnam: A  
772 plot-scale study. *Geoderma* 232–234, 352–362.  
773 <https://doi.org/10.1016/j.geoderma.2014.05.011>
- 774 Awadhwai, N.K., Thierstein, G.E., 1985. Soil crust and its impact on crop establishment: A  
775 review. *Soil Tillage Res.* 5, 289–302. [https://doi.org/10.1016/0167-1987\(85\)90021-2](https://doi.org/10.1016/0167-1987(85)90021-2)
- 776 Barthès, B., Roose, E., 2002. Aggregate stability as an indicator of soil susceptibility to runoff  
777 and erosion; validation at several levels. *Catena* 47, 133–149. [https://doi.org/10.1016/S0341-8162\(01\)00180-1](https://doi.org/10.1016/S0341-8162(01)00180-1)  
778

- 779 Baruah, S., Ramalingam, K., Kannan, B., Kaliaperumal, R., 2019. Soil erodibility estimation and  
780 its correlation with soil properties in Coimbatore district Soil erodibility estimation and its  
781 correlation with soil properties in Coimbatore district. *Int. J. Chem. Stud.* 7, 3327–3332.
- 782 Benjeddou, O., Soussi, C., Jedidi, M., Benali, M., 2017. Experimental and theoretical study of the  
783 effect of the particle size of limestone fillers on the rheology of self-compacting concrete. *J.*  
784 *Build. Eng.* 10, 32–41. <https://doi.org/10.1016/J.JOBE.2017.02.003>
- 785 Brakensiek, D.L., Rawls, W.J., 1994. Soil containing rock fragments: effects on infiltration.  
786 *CATENA* 23, 99–110. [https://doi.org/10.1016/0341-8162\(94\)90056-6](https://doi.org/10.1016/0341-8162(94)90056-6)
- 787 Burch, G.J., Moore, I.D., Burns, J., 1989. Soil hydrophobic effects on infiltration and catchment  
788 runoff. *Hydrol. Process.* 3, 211–222. <https://doi.org/10.1002/HYP.3360030302>
- 789 Buttle, J.M., Turcotte, D.S., 1999. Runoff processes on a forested slope on the Canadian shield.  
790 *Nord. Hydrol.* 30, 1–20. <https://doi.org/10.2166/nh.1999.0001>
- 791 Cerdà, A., Lucas-Borja, M.E., Franch-Pardo, I., Úbeda, X., Novara, A., López-Vicente, M.,  
792 Popović, Z., Pulido, M., 2021. The role of plant species on runoff and soil erosion in a  
793 Mediterranean shrubland. *Sci. Total Environ.* 799, 149218.  
794 <https://doi.org/10.1016/j.scitotenv.2021.149218>
- 795 Cerdan, O., Govers, G., Le Bissonnais, Y., Van Oost, K., Poesen, J., Saby, N., Gobin, A., Vacca,  
796 A., Quinton, J., Auerswald, K., Klik, A., Kwaad, F.J.P.M., Raclot, D., Ionita, I., Rejman, J.,  
797 Rousseva, S., Muxart, T., Roxo, M.J., Dostal, T., 2010. Rates and spatial variations of soil  
798 erosion in Europe: A study based on erosion plot data. *Geomorphology* 122, 167–177.  
799 <https://doi.org/10.1016/j.geomorph.2010.06.011>
- 800 Chmelová, R., Šarapatka, B., 2002. Soil erosion by water: Contemporary research methods and  
801 their use. *Geographica* 37, 23–30.
- 802 Chou, C.S., Yang, R.Y., Chen, J.H., Chou, S.W., 2010. The optimum conditions for preparing the  
803 lead-free piezoelectric ceramic of Bi<sub>0.5</sub>Na<sub>0.5</sub>TiO<sub>3</sub> using the Taguchi method. *Powder*  
804 *Technol.* 199, 264–271. <https://doi.org/10.1016/j.powtec.2010.01.015>
- 805 Cox, N.J., Warburton, J., Armstrong, A., Holliday, V.J., 2008. Fitting concentration and load  
806 rating curves with generalized linear models. *Earth Surf. Process. Landforms* 33, 25–39.  
807 <https://doi.org/10.1002/ESP.1523>
- 808 De Jonge, L.W., Moldrup, P., Jacobsen, O.H., 2007. Soil-water content dependency of water  
809 repellency in soils. *Soil Sci.* 172, 577–588. <https://doi.org/10.1097/SS.0B013E318065C090>
- 810 Defersha, M.B., Melesse, A.M., 2012. Effect of rainfall intensity, slope and antecedent moisture  
811 content on sediment concentration and sediment enrichment ratio. *Catena* 90, 47–52.  
812 <https://doi.org/10.1016/j.catena.2011.11.002>
- 813 Deng, L., Zhang, L., Fan, X., Sun, T., Fei, K., Ni, L., 2019. Effects of rainfall intensity and slope  
814 gradient on runoff and sediment yield from hillslopes with weathered granite. *Environ. Sci.*  
815 *Pollut. Res.* 26, 32559–32573. <https://doi.org/10.1007/s11356-019-06486-z>
- 816 Donjadee, S., Chinnarasri, C., 2012. Effects of rainfall intensity and slope gradient on the  
817 application of vetiver grass mulch in soil and water conservation. *Int. J. Sediment Res.* 27,  
818 168–177. [https://doi.org/10.1016/S1001-6279\(12\)60025-0](https://doi.org/10.1016/S1001-6279(12)60025-0)

- 819 Duiker, S.W., Flanagan, D.C., Lal, R., 2001. Erodibility and infiltration characteristics of five  
820 major soils of southwest Spain. *Catena* 45, 103–121. <https://doi.org/10.1016/S0341->  
821 8162(01)00145-X
- 822 Dunj6, G., Pardini, G., Gispert, M., 2004. The role of land use-land cover on runoff generation  
823 and sediment yield at a microplot scale, in a small Mediterranean catchment. *J. Arid*  
824 *Environ.* 57, 239–256. [https://doi.org/10.1016/S0140-1963\(03\)00097-1](https://doi.org/10.1016/S0140-1963(03)00097-1)
- 825 Ekwue, E.I., 1990. Organic-matter effects on soil strength properties. *Soil Tillage Res.* 16, 289–  
826 297. [https://doi.org/10.1016/0167-1987\(90\)90102-J](https://doi.org/10.1016/0167-1987(90)90102-J)
- 827 Eslamian, S., 2014. Handbook of engineering hydrology: Modeling, climate change, and  
828 variability. *Handb. Eng. Hydrol. Model. Clim. Chang. Var.* 1–615.  
829 <https://doi.org/10.1201/b16683>
- 830 Fern6ndez-G6lvez, J., Barahona, E., Mingorance, M.D., 2008. Measurement of infiltration in  
831 small field plots by a portable rainfall simulator: Application to trace-element mobility.  
832 *Water. Air. Soil Pollut.* 191, 257–264. <https://doi.org/10.1007/s11270-008-9622-2>
- 833 Gomi, T., Sidle, R.C., Ueno, M., Miyata, S., Kosugi, K., 2008. Characteristics of overland flow  
834 generation on steep forested hillslopes of central Japan. *J. Hydrol.* 361, 275–290.  
835 <https://doi.org/10.1016/J.JHYDROL.2008.07.045>
- 836 Grismer, M.E., 2012. Mod6lisation de l'6rosion pour la gestion des terres dans le bassin du lac  
837 Tahoe, Etats-Unis: scalance depuis les parcelles jusqu'aux bassins versants forestiers.  
838 *Hydrol. Sci. J.* 57, 878–900. <https://doi.org/10.1080/02626667.2012.685170>
- 839 Gross, C.M., Angle, J.S., Hill, R.L., Welterlen, M.S., 1991. Runoff and Sediment Losses from  
840 Tall Fescue under Simulated Rainfall. *J. Environ. Qual.* 20, 604–607.  
841 <https://doi.org/10.2134/jeq1991.00472425002000030017x>
- 842 Guidry, A.R., Schindler, F. V., German, D.R., Gelderman, R.H., Gerwing, J.R., 2006. Using  
843 Simulated Rainfall to Evaluate Field and Indoor Surface Runoff Phosphorus Relationships.  
844 *J. Environ. Qual.* 35, 2236–2243. <https://doi.org/10.2134/jeq2006.0156>
- 845 Guo, Z., Ma, M., Cai, C., Wu, Y., 2018. Combined effects of simulated rainfall and overland  
846 flow on sediment and solute transport in hillslope erosion. *J. Soils Sediments* 18, 1120–  
847 1132. <https://doi.org/10.1007/s11368-017-1868-0>
- 848 He, Z., Jia, G., Liu, Z., Zhang, Z., Yu, X., Xiao, P., 2020. Field studies on the influence of  
849 rainfall intensity, vegetation cover and slope length on soil moisture infiltration on typical  
850 watersheds of the Loess Plateau, China. *Hydrol. Process.* 34, 4904–4919.  
851 <https://doi.org/10.1002/hyp.13892>
- 852 Heiskanen, J., 2008. Comparison of three methods for determining the particle density of soil  
853 with liquid pycnometers. <http://dx.doi.org/10.1080/00103629209368633> 23, 841–846.  
854 <https://doi.org/10.1080/00103629209368633>
- 855 Hermansen, C., Moldrup, P., M6ller, K., Knadel, M., Jonge, L.W. de, 2019. The Relation  
856 between Soil Water Repellency and Water Content Can Be Predicted by Vis-NIR  
857 Spectroscopy. *Soil Sci. Soc. Am. J.* 83, 1616–1627.  
858 <https://doi.org/10.2136/SSSAJ2019.03.0092>

- 859 Herweg, K., Ludi, E., 1999. The performance of selected soil and water conservation measures -  
860 Case studies from Ethiopia and Eritrea. *Catena* 36, 99–114. <https://doi.org/10.1016/S0341->  
861 8162(99)00004-1
- 862 Holz, M., Augustin, J., 2021. Erosion effects on soil carbon and nitrogen dynamics on cultivated  
863 slopes: A meta-analysis. *Geoderma* 397, 115045.  
864 <https://doi.org/10.1016/J.GEODERMA.2021.115045>
- 865 Hrabovský, A., Dlapa, P., Cerdà, A., Kollár, J., 2020. The impacts of vineyard afforestation on  
866 soil properties, water repellency and near-saturated infiltration in the little carpathians  
867 mountains. *Water* 12, 2550. <https://doi.org/10.3390/w12092550>
- 868 Huang, R., Huang, L., He, B., Zhou, L., Wang, F., 2012. Effects of slope forest and grass  
869 vegetation on reducing rainfall-runoff erosivity in Three Gorges Reservoir Region. *Nongye*  
870 *Gongcheng Xuebao/Transactions Chinese Soc. Agric. Eng.* 28, 70–76.  
871 <https://doi.org/10.3969/j.issn.1002-6819.2012.09.012>
- 872 Ihinegbu, C., Ogunwumi, T., 2021. Multi-criteria modelling of drought: a study of Brandenburg  
873 Federal State, Germany. *Model. Earth Syst. Environ.* 1, 3. <https://doi.org/10.1007/s40808->  
874 021-01197-2
- 875 Issaka, S., Ashraf, M.A., 2017. Impact of soil erosion and degradation on water quality: a review.  
876 <https://doi.org/10.1080/24749508.2017.1301053> 1, 1–11.  
877 <https://doi.org/10.1080/24749508.2017.1301053>
- 878 J. R. Williams, C. A. Jones, P. T. Dyke, 1984. A Modeling Approach to Determining the  
879 Relationship Between Erosion and Soil Productivity. *Trans. ASAE* 27, 0129–0144.  
880 <https://doi.org/10.13031/2013.32748>
- 881 Jahun, B.G., Ibrahim, R., Dlamini, N.S., Musa, S.M., 2015. Review of Soil Erosion Assessment  
882 using RUSLE Model and GIS. *J. Biol. Agric. Healthc.* 5, 36–47.
- 883 Jebari, S., Berndtsson, R., Bahri, A., Boufaroua, M., 2008. Exceptional Rainfall Characteristics  
884 Related to Erosion Risk in Semiarid Tunisia. *Open Hydrol. J.* 2, 25–33.  
885 <https://doi.org/10.2174/1874378100802010025>
- 886 Jourgholami, M., Karami, S., Tavankar, F., Lo Monaco, A., Picchio, R., 2021. Effects of slope  
887 gradient on runoff and sediment yield on machine-induced compacted soil in temperate  
888 forests. *Forests* 12, 1–19. <https://doi.org/10.3390/f12010049>
- 889 Jourgholami, M., Labelle, E.R., 2020. Effects of plot length and soil texture on runoff and  
890 sediment yield occurring on machine-trafficked soils in a mixed deciduous forest. *Ann. For.*  
891 *Sci.* 77, 1–11. <https://doi.org/10.1007/s13595-020-00938-0>
- 892 Kamphorst, A., 1987. A small rainfall simulator for the determination of soil erodibility.  
893 *Netherlands J. Agric. Sci.* 35, 407–415. <https://doi.org/10.18174/NJAS.V35I3.16735>
- 894 Kandel, D.D., Western, A.W., Grayson, R.B., Turrall, H.N., 2004. Process parameterization and  
895 temporal scaling in surface runoff and erosion modelling. *Hydrol. Process.* 18, 1423–1446.  
896 <https://doi.org/10.1002/hyp.1421>
- 897 Keating, B.A., Carberry, P.S., Hammer, G.L., Probert, M.E., Robertson, M.J., Holzworth, D.,  
898 Huth, N.I., Hargreaves, J.N.G., Meinke, H., Hochman, Z., McLean, G., Verburg, K., Snow,

899 V., Dimes, J.P., Silburn, M., Wang, E., Brown, S., Bristow, K.L., Asseng, S., Chapman, S.,  
900 McCown, R.L., Freebairn, D.M., Smith, C.J., 2003. An overview of APSIM, a model  
901 designed for farming systems simulation. *Eur. J. Agron.* 18, 267–288.  
902 [https://doi.org/10.1016/S1161-0301\(02\)00108-9](https://doi.org/10.1016/S1161-0301(02)00108-9)

903 Kirkby, M.J., Jones, R., Irvine, B., Gobin, A., Govers, G., Cerdan, O., Rompaey, A.J.J. Van, Le  
904 Bissonnais, Y., Daroussin, J., King, D., Montanarella, L., Grimm, M., Vieillefont, V.,  
905 Puigdefabregas, J., Boer, M., Kosmas, C., Yassoglou, N., Tsara, M., Mantel, S., Lynden,  
906 G.J. Van, Huting, J., 2004. Pan-European Soil Erosion Risk Assessment: The PESERA  
907 Map, Version 1 October 2003. Explanation of Special Publication Ispra 2004 No.73  
908 (S.P.I.04.73), European Soil Bureau Research Report. Luxembourg.

909 Knadel, M., Masís-Meléndez, F., De Jonge, L.W., Moldrup, P., Arthur, E., Greve, M.H., 2016.  
910 Assessing Soil Water Repellency of a Sandy Field with Visible near Infrared Spectroscopy:  
911 <http://dx.doi.org/10.1255/jnirs.1188> 24, 215–224. <https://doi.org/10.1255/JNIRS.1188>

912 Knisel, W.G., Nicks, A.D., 1981. CREAMS: A Field Scale Model for Chemicals, Runoff, and  
913 Erosion from Agriculture Management System, 26th ed, United States. Science and  
914 Education Administration. Dept. of Agriculture, Science and Education Administration.

915 Kort, J., Collins, M., Ditsch, D., 1998. A review of soil erosion potential associated with biomass  
916 crops. *Biomass and Bioenergy* 14, 351–359. [https://doi.org/10.1016/S0961-9534\(97\)10071-](https://doi.org/10.1016/S0961-9534(97)10071-X)  
917 X

918 Krisnayanti, D.S., Bunganaen, W., Frans, J.H., Seran, Y.A., Legono, D., 2021. Curve number  
919 estimation for ungauged watershed in semiarid region. *Civ. Eng. J.* 7, 1070–1083.  
920 <https://doi.org/10.28991/CEJ-2021-03091711>

921 Krysanova, V., Hattermann, F., Wechsung, F., 2007. Implications of complexity and uncertainty  
922 for integrated modelling and impact assessment in river basins. *Environ. Model. Softw.* 22,  
923 701–709. <https://doi.org/10.1016/j.envsoft.2005.12.029>

924 Kühn, P., 2003. Micromorphology and Late Glacial/Holocene genesis of Luvisols in  
925 Mecklenburg–Vorpommern (NE-Germany). *CATENA* 54, 537–555.  
926 [https://doi.org/10.1016/S0341-8162\(03\)00129-2](https://doi.org/10.1016/S0341-8162(03)00129-2)

927 Kusumandari, A., Satriagasa, M.C., Hadi Purwanto, R., Widayanti, W.T., 2021. Erosion  
928 Measurement by Using Rainfall Simulator at Grass Soil and after Harvested Soil in  
929 Wanagama, in: *IOP Conference Series: Earth and Environmental Science*. IOP Publishing.  
930 <https://doi.org/10.1088/1755-1315/810/1/012053>

931 L. D. Meyer, 1981. How Rain Intensity Affects Interrill Erosion. *Trans. ASAE* 24, 1472–1475.  
932 <https://doi.org/10.13031/2013.34475>

933 Lasanta, T., García-Ruiz, J.M., Pérez-Rontomé, C., Sancho-Marcén, C., 2000. Runoff and  
934 sediment yield in a semi-arid environment: The effect of land management after farmland  
935 abandonment. *Catena* 38, 265–278. [https://doi.org/10.1016/S0341-8162\(99\)00079-X](https://doi.org/10.1016/S0341-8162(99)00079-X)

936 Li, T., Zhao, L., Duan, H., Yang, Y., Wang, Y., Wu, F., 2020. Exploring the interaction of  
937 surface roughness and slope gradient in controlling rates of soil loss from sloping farmland  
938 on the Loess Plateau of China. *Hydrol. Process.* 34, 339–354.  
939 <https://doi.org/10.1002/HYP.13588>

- 940 Li, Y., Zhang, F., Yang, M., Zhang, J., Xie, Y., 2019. Impacts of biochar application rates and  
941 particle sizes on runoff and soil loss in small cultivated loess plots under simulated rainfall.  
942 *Sci. Total Environ.* 649, 1403–1413. <https://doi.org/10.1016/j.scitotenv.2018.08.415>
- 943 Li, Z., Liu, C., Dong, Y., Chang, X., Nie, X., Liu, L., Xiao, H., Lu, Y., Zeng, G., 2017. Response  
944 of soil organic carbon and nitrogen stocks to soil erosion and land use types in the Loess  
945 hilly–gully region of China. *Soil Tillage Res.* 166, 1–9.  
946 <https://doi.org/10.1016/j.still.2016.10.004>
- 947 Li, Z., Yu, X., 2012. Characteristics of surface runoff and its influencing factors on slope scale in  
948 rocky mountain area of northern Hebei province. *Nongye Gongcheng Xuebao/Transactions*  
949 *Chinese Soc. Agric. Eng.* 28, 109–116. [https://doi.org/10.3969/J.ISSN.1002-](https://doi.org/10.3969/J.ISSN.1002-6819.2012.17.016)  
950 [6819.2012.17.016](https://doi.org/10.3969/J.ISSN.1002-6819.2012.17.016)
- 951 Lin, J., Zhu, G., Wei, J., Jiang, F., Wang, M. kuang, Huang, Y., 2018. Mulching effects on  
952 erosion from steep slopes and sediment particle size distributions of gully colluvial deposits.  
953 *CATENA* 160, 57–67. <https://doi.org/10.1016/J.CATENA.2017.09.003>
- 954 Liu, D., She, D., Yu, S., Shao, G., Chen, D., 2015. Rainfall intensity and slope gradient effects on  
955 sediment losses and splash from a saline-sodic soil under coastal reclamation. *Catena* 128,  
956 54–62. <https://doi.org/10.1016/j.catena.2015.01.022>
- 957 Liu, Singh, 2004. Effect of Microtopography, Slope Length and Gradient, and Vegetative Cover  
958 on Overland Flow through Simulation. *J. Hydrol. Eng.* 9, 375–382.  
959 [https://doi.org/10.1061/\(ASCE\)1084-0699\(2004\)9:5\(375\)](https://doi.org/10.1061/(ASCE)1084-0699(2004)9:5(375))
- 960 Liu, Y., Xin, Y., Xie, Y., Wang, W., 2019. Effects of slope and rainfall intensity on runoff and  
961 soil erosion from furrow diking under simulated rainfall. *Catena* 177, 92–100.  
962 <https://doi.org/10.1016/j.catena.2019.02.004>
- 963 Loch, R.J., 2000. Effects of vegetation cover on runoff and erosion under simulated rain and  
964 overland flow on a rehabilitated site on the Meandu Mine, Tarong, Queensland. *Soil Res.*  
965 38, 299–312. <https://doi.org/10.1071/SR99030>
- 966 Lu, J., Zheng, F., Li, G., Bian, F., An, J., 2016. The effects of raindrop impact and runoff  
967 detachment on hillslope soil erosion and soil aggregate loss in the Mollisol region of  
968 Northeast China. *Soil Tillage Res.* 161, 79–85. <https://doi.org/10.1016/J.STILL.2016.04.002>
- 969 M. Sheklabadi, H. Khademi, A. H. Charkhabi, 2012. Runoff and Sediment Yield in Soils  
970 Developed on Different Parent Materials in the Golabad Watershed, Ardestan. *J. Sci.*  
971 *Technol. Agric. Nat. Resour.* 7, 101–245.
- 972 Meena, R.S., Lal, R., Yadav, G.S., 2020. Long-term impacts of topsoil depth and amendments on  
973 soil physical and hydrological properties of an Alfisol in central Ohio, USA. *Geoderma* 363,  
974 114164. <https://doi.org/10.1016/J.GEODERMA.2019.114164>
- 975 Meng, Q., Fu, B., Tang, X., Ren, H., 2007. Effects of land use on phosphorus loss in the hilly  
976 area of the Loess Plateau, China. *Environ. Monit. Assess.* 2007 1391 139, 195–204.  
977 <https://doi.org/10.1007/S10661-007-9826-8>
- 978 Meyer, L.D., Harmon, W.C., 1989. How row-sideslope length and steepness affect sideslope  
979 erosion. *Trans. Am. Soc. Agric. Eng.* 32, 639–644. <https://doi.org/10.13031/2013.31050>

- 980 Michel, E., Majdalani, S., Di-Pietro, L., 2014. A novel conceptual framework for long-term  
981 leaching of autochthonous soil particles during transient flow. *Eur. J. Soil Sci.* 65, 336–347.  
982 <https://doi.org/10.1111/ejss.12135>
- 983 Mohamadi, M.A., Kavian, A., 2015. Effects of rainfall patterns on runoff and soil erosion in field  
984 plots. *Int. Soil Water Conserv. Res.* 3, 273–281. <https://doi.org/10.1016/j.iswcr.2015.10.001>
- 985 Nassif, S.H., Wilson, E.M., 1975. The influence of slope and rain intensity on runoff and  
986 infiltration. *Hydrol. Sci. Bull.* 20, 539–553. <https://doi.org/10.1080/02626667509491586>
- 987 Nearing, M.A., Simanton, J.R., Norton, L.D., Bulygin, S.J., Stone, J., 1999. Soil erosion by  
988 surface water flow on a stony, semiarid hillslope. *Earth Surf. Process. Landforms* 24, 677–  
989 686. [https://doi.org/10.1002/\(SICI\)1096-9837\(199908\)24:8<677::AID-ESP981>3.0.CO;2-1](https://doi.org/10.1002/(SICI)1096-9837(199908)24:8<677::AID-ESP981>3.0.CO;2-1)
- 990 Nunes, A.N., de Almeida, A.C., Coelho, C.O.A., 2011. Impacts of land use and cover type on  
991 runoff and soil erosion in a marginal area of Portugal. *Appl. Geogr.* 31, 687–699.  
992 <https://doi.org/10.1016/J.APGEOG.2010.12.006>
- 993 Ouyang, W., Wu, Y., Hao, Z., Zhang, Q., Bu, Q., Gao, X., 2018. Combined impacts of land use  
994 and soil property changes on soil erosion in a mollisol area under long-term agricultural  
995 development. *Sci. Total Environ.* 613–614, 798–809.  
996 <https://doi.org/10.1016/J.SCITOTENV.2017.09.173>
- 997 P.U., I., A.A., O., O.C., C., I.I., E., M.M., M., 2017. Soil Erosion: A Review of Models and  
998 Applications. *Int. J. Adv. Eng. Res. Sci.* 4, 138–150. <https://doi.org/10.22161/ijaers.4.12.22>
- 999 Panagos, P., Katsoyiannis, A., 2019. Soil erosion modelling: The new challenges as the result of  
1000 policy developments in Europe. *Environ. Res.* 172, 470–474.  
1001 <https://doi.org/10.1016/j.envres.2019.02.043>
- 1002 Pandey, A., Chowdary, V.M., Mal, B.C., 2007. Identification of critical erosion prone areas in the  
1003 small agricultural watershed using USLE, GIS and remote sensing. *Water Resour. Manag.*  
1004 21, 729–746. <https://doi.org/10.1007/s11269-006-9061-z>
- 1005 Parr, W.C., Taguchi, G., 1989. Introduction to Quality Engineering: Designing Quality into  
1006 Products and Processes. *Technometrics* 31, 255. <https://doi.org/10.2307/1268824>
- 1007 Peng, T., Wang, S. jie, 2012. Effects of land use, land cover and rainfall regimes on the surface  
1008 runoff and soil loss on karst slopes in southwest China. *CATENA* 90, 53–62.  
1009 <https://doi.org/10.1016/J.CATENA.2011.11.001>
- 1010 Poulénard, J., Podwojewski, P., Janeau, J.L., Collinet, J., 2001. Runoff and soil erosion under  
1011 rainfall simulation of Andisols from the Ecuadorian Páramo: Effect of tillage and burning.  
1012 *Catena* 45, 185–207. [https://doi.org/10.1016/S0341-8162\(01\)00148-5](https://doi.org/10.1016/S0341-8162(01)00148-5)
- 1013 Rainfall simulator - Field measurement equipment | Eijkelkamp [WWW Document], 2018. URL  
1014 <https://en.eijkelkamp.com/products/field-measurement-equipment/rainfall-simulator.html>  
1015 (accessed 10.20.21).
- 1016 Ramezanpour, H., Esmaeilnejad, L., Akbarzadeh, A., 2010. Influence of soil physical and  
1017 mineralogical properties on erosion variations in Marlylands of Southern Guilan Province,  
1018 Iran. *Int. J. Phys. Sci.* 5, 365–378. <https://doi.org/10.5897/IJPS.9000311>

- 1019 Ramos, M.C., Lizaga, I., Gaspar, L., Quijano, L., Navas, A., 2019. Effects of rainfall intensity  
1020 and slope on sediment, nitrogen and phosphorous losses in soils with different use and soil  
1021 hydrological properties. *Agric. Water Manag.* 226, 105789.  
1022 <https://doi.org/10.1016/j.agwat.2019.105789>
- 1023 Raza, A., Ahrends, H., Habib-Ur-Rahman, M., Gaiser, T., 2021. Modeling Approaches to Assess  
1024 Soil Erosion by Water at the Field Scale with Special Emphasis on Heterogeneity of Soils  
1025 and Crops. *L.* 2021, Vol. 10, Page 422 10, 422. <https://doi.org/10.3390/LAND10040422>
- 1026 Renard, K.G., Foster, G.R., Weesies, G.A., Porter, J.P., 1991. RUSLE: revised universal soil loss  
1027 equation. *J. Soil Water Conserv.* 46, 30–33.
- 1028 Rieke-Zapp, D.H., Nearing, M.A., 2005. Slope Shape Effects on Erosion: A Laboratory Study.  
1029 *Soil Sci. Soc. Am. J.* 69, 1463–1471. <https://doi.org/10.2136/sssaj2005.0015>
- 1030 Roth, C.H., Vieira, M.J., Derpsch, R., Meyer, B., Frede, H. -G, 1987. Infiltrability of an Oxisol in  
1031 Paraná, Brazil as Influenced by Different Crop Rotations. *J. Agron. Crop Sci.* 159, 186–191.  
1032 <https://doi.org/10.1111/j.1439-037X.1987.tb00084.x>
- 1033 Sadeghi, S.H., Kiani Harchegani, M., Asadi, H., 2017. Variability of particle size distributions of  
1034 upward/downward splashed materials in different rainfall intensities and slopes. *Geoderma*  
1035 290, 100–106. <https://doi.org/10.1016/j.geoderma.2016.12.007>
- 1036 Sepaskhah, A.R., Bazrafshan-Jahromi, A.R., 2006. Controlling Runoff and Erosion in Sloping  
1037 Land with Polyacrylamide under a Rainfall Simulator. *Biosyst. Eng.* 93, 469–474.  
1038 <https://doi.org/10.1016/j.biosystemseng.2006.01.003>
- 1039 Sharpley, A., Kleinman, P., 2003. Effect of Rainfall Simulator and Plot Scale on Overland Flow  
1040 and Phosphorus Transport. *J. Environ. Qual.* 32, 2172–2179.  
1041 <https://doi.org/10.2134/jeq2003.2172>
- 1042 Sivaiah, P., Chakradhar, D., 2019. Modeling and optimization of sustainable manufacturing  
1043 process in machining of 17-4 PH stainless steel. *Meas. J. Int. Meas. Confed.* 134, 142–152.  
1044 <https://doi.org/10.1016/j.measurement.2018.10.067>
- 1045 Sosa-Pérez, G., MacDonald, L.H., 2017. Effects of closed roads, traffic, and road  
1046 decommissioning on infiltration and sediment production: A comparative study using  
1047 rainfall simulations. *CATENA* 159, 93–105.  
1048 <https://doi.org/10.1016/J.CATENA.2017.08.004>
- 1049 Srinivasan, M.S., Kleinman, P.J.A., Sharpley, A.N., Buob, T., Gburek, W.J., 2007. Hydrology of  
1050 Small Field Plots Used to Study Phosphorus Runoff under Simulated Rainfall. *J. Environ.*  
1051 *Qual.* 36, 1833–1842. <https://doi.org/10.2134/jeq2007.0017>
- 1052 Sukartaatmadja, S., Sato, Y., Yamaji, E., Ishikawa, M., 2003. The Effect of Rainfall Intensity on  
1053 Soil Erosion and Runoff for Latosol Soil in Indonesia. *Indones. J. Agron.* 31.  
1054 <https://doi.org/10.24831/jai.v31i2.1469>
- 1055 Sun, L., Zhou, J.L., Cai, Q., Liu, S., Xiao, J., 2021. Comparing surface erosion processes in four  
1056 soils from the Loess Plateau under extreme rainfall events. *Int. Soil Water Conserv. Res.* 9,  
1057 520–531. <https://doi.org/10.1016/J.ISWCR.2021.06.008>
- 1058 Syvitski, J.P.M., Kettner, A.J., 2008. Scaling sediment flux across landscapes. *IAHS-AISH Publ.*

- 1059 149–156.
- 1060 Taguchi, G., 1987. *The System of Experimental Design: Engineering Methods to Optimize*  
1061 *Quality and Minimize Costs*, 1st ed, Response. Quality Resources.
- 1062 Taguchi, G., 1986. *Introduction to quality engineering : designing quality into products and*  
1063 *processes*. Quality Resources.
- 1064 Tong Li, Dong, J., Yuan, W., 2020. Effects of Precipitation and Vegetation Cover on Annual  
1065 Runoff and Sediment Yield in Northeast China: A Preliminary Analysis. *Water Resour.* 47,  
1066 491–505. <https://doi.org/10.1134/S0097807820030173/FIGURES/10>
- 1067 Václavík, T., Lautenbach, S., Kuemmerle, T., Seppelt, R., 2013. Mapping global land system  
1068 archetypes. *Glob. Environ. Chang.* 23, 1637–1647.  
1069 <https://doi.org/10.1016/j.gloenvcha.2013.09.004>
- 1070 Van Dijk, P.M., Van Der Zipp, M., Kwaad, F.J.P.M., 1996. Soil erodibility parameters under  
1071 various cropping systems of maize. *Hydrol. Process.* 10, 1061–1067.  
1072 [https://doi.org/10.1002/\(SICI\)1099-1085\(199608\)10:8<1061::AID-HYP411>3.0.CO;2-V](https://doi.org/10.1002/(SICI)1099-1085(199608)10:8<1061::AID-HYP411>3.0.CO;2-V)
- 1073 Viney, N.R., Sivapalan, M., 1999. A conceptual model of sediment transport: Application to the  
1074 Avon River Basin in Western Australia. *Hydrol. Process.* 13, 727–743.  
1075 [https://doi.org/10.1002/\(SICI\)1099-1085\(19990415\)13:5<727::AID-HYP776>3.0.CO;2-D](https://doi.org/10.1002/(SICI)1099-1085(19990415)13:5<727::AID-HYP776>3.0.CO;2-D)
- 1076 Wang, Y., Fan, J., Cao, L., Liang, Y., 2016. Infiltration and Runoff Generation Under Various  
1077 Cropping Patterns in the Red Soil Region of China. *L. Degrad. Dev.* 27, 83–91.  
1078 <https://doi.org/10.1002/ldr.2460>
- 1079 Warrington, D., Shainberg, I., Agassi, M., Morin, J., 1989. Slope and Phosphogypsum's Effects  
1080 on Runoff and Erosion. *Soil Sci. Soc. Am. J.* 53, 1201–1205.  
1081 <https://doi.org/10.2136/sssaj1989.03615995005300040035x>
- 1082 Wu, L., Peng, M., Qiao, S., Ma, X. yi, 2018a. Effects of rainfall intensity and slope gradient on  
1083 runoff and sediment yield characteristics of bare loess soil. *Environ. Sci. Pollut. Res.*  
1084 <https://doi.org/10.1007/s11356-017-0713-8>
- 1085 Wu, L., Qiao, S., Peng, M., Ma, X., 2018b. Coupling loss characteristics of runoff-sediment-  
1086 adsorbed and dissolved nitrogen and phosphorus on bare loess slope. *Environ. Sci. Pollut.*  
1087 *Res.* 25, 14018–14031. <https://doi.org/10.1007/s11356-018-1619-9>
- 1088 Yan, Y., Dai, Q., Yuan, Y., Peng, X., Zhao, L., Yang, J., 2018. Effects of rainfall intensity on  
1089 runoff and sediment yields on bare slopes in a karst area, SW China. *Geoderma* 330, 30–40.  
1090 <https://doi.org/10.1016/j.geoderma.2018.05.026>
- 1091 Yost, J.L., Hartemink, A.E., 2019. Soil organic carbon in sandy soils: A review. *Adv. Agron.*  
1092 158, 217–310. <https://doi.org/10.1016/BS.AGRON.2019.07.004>
- 1093 Yusuf, K., Omokore, S., Oyebo, O., Adebayo, K., 2016. Effect of vegetative cover and slope  
1094 on soil loss by erosion using rainfall simulator. *J. Res. For. Wildl. Environ.* 8, 45–52.
- 1095 Zambon, N., Johannsen, L.L., Strauss, P., Dostal, T., Zumr, D., Cochrane, T.A., Klik, A., 2021.  
1096 Splash erosion affected by initial soil moisture and surface conditions under simulated  
1097 rainfall. *Catena* 196, 104827. <https://doi.org/10.1016/j.catena.2020.104827>

- 1098 Zapata, N., Salvador, R., Latorre, B., Paniagua, P., Medina, E.T., Playán, E., 2021. Effect of a  
 1099 growing maize canopy on solid-set sprinkler irrigation: kinetic energy dissipation and water  
 1100 partitioning. *Irrig. Sci.* 39, 329–346. [https://doi.org/10.1007/S00271-020-00713-](https://doi.org/10.1007/S00271-020-00713-Z)  
 1101 [Z/FIGURES/10](https://doi.org/10.1007/S00271-020-00713-Z)
- 1102 Zhang, F., Yang, M., Li, Z., 2015. Feasibility analysis of replacing full factorial design with  
 1103 Taguchi method in mini-plot soil erosion experiments. *Nongye Gongcheng*  
 1104 *Xuebao/Transactions Chinese Soc. Agric. Eng.* 31, 1–9.  
 1105 <https://doi.org/10.11975/J.ISSN.1002-6819.2015.13.001>
- 1106 Zhang, J.H., Wang, Y., Li, F.C., 2015. Soil organic carbon and nitrogen losses due to soil erosion  
 1107 and cropping in a sloping terrace landscape. *Soil Res.* 53, 87–96.  
 1108 <https://doi.org/10.1071/SR14151>
- 1109 Zhao, Q., Li, D., Zhuo, M., Guo, T., Liao, Y., Xie, Z., 2015. Effects of rainfall intensity and slope  
 1110 gradient on erosion characteristics of the red soil slope. *Stoch. Environ. Res. Risk Assess.*  
 1111 29, 609–621. <https://doi.org/10.1007/S00477-014-0896-1>/[FIGURES/6](https://doi.org/10.1007/S00477-014-0896-1)
- 1112 Zhong, R.-L., Zhang, P.-C., 2011. Experimental Study on Characteristics of Runoff and Erosional  
 1113 Sediment Yield on Purple Soil Slope. *J. yangtze river Sci. Res. Inst.* 28, 22–27.
- 1114 Ziadat, F.M., Taimeh, A.Y., 2013a. Effect of rainfall intensity, slope, land use and antecedent soil  
 1115 moisture on soil erosion in an arid environment. *L. Degrad. Dev.* 24, 582–590.  
 1116 <https://doi.org/10.1002/ldr.2239>
- 1117 Ziadat, F.M., Taimeh, A.Y., 2013b. Effect of rainfall intensity, slope, land use and antecedent soil  
 1118 moisture on soil erosion in an arid environment. *L. Degrad. Dev.* 24, 582–590.  
 1119 <https://doi.org/10.1002/ldr.2239>
- 1120 Zuazo, V.H.D., Pleguezuelo, C.R.R., 2008. Soil-erosion and runoff prevention by plant covers. A  
 1121 review. *Agron. Sustain. Dev.* <https://doi.org/10.1051/agro:2007062>
- 1122